molecules

MDPI

Review

Intramolecular Hydrogen Bonding Involving Organic Fluorine: NMR Investigations Corroborated by DFT-Based Theoretical Calculations

Sandeep Kumar Mishra and N. Suryaprakash *

NMR Research Centre, Solid State and Structural Chemistry Unit, Indian Institute of Science, Bangalore 560012, India; sand2epmishra@gmail.com

* Correspondence: suryaprakash1703@gmail.com; Tel.: +80-2293-7344 or +80-2293-3300 or +91-9845124802; Fax: +91-2360-1550

Academic Editor: Steve Scheiner

Received: 31 January 2017; Accepted: 2 March 2017; Published: 7 March 2017

Abstract: The combined utility of many one and two dimensional NMR methodologies and DFT-based theoretical calculations have been exploited to detect the intramolecular hydrogen bond (HB) in number of different organic fluorine-containing derivatives of molecules, viz. benzanilides, hydrazides, imides, benzamides, and diphenyloxamides. The existence of two and three centered hydrogen bonds has been convincingly established in the investigated molecules. The NMR spectral parameters, viz., coupling mediated through hydrogen bond, one-bond NH scalar couplings, physical parameter dependent variation of chemical shifts of NH protons have paved the way for understanding the presence of hydrogen bond involving organic fluorine in all the investigated molecules. The experimental NMR findings are further corroborated by DFT-based theoretical calculations including NCI, QTAIM, MD simulations and NBO analysis. The monitoring of H/D exchange with NMR spectroscopy established the effect of intramolecular HB and the influence of electronegativity of various substituents on the chemical kinetics in the number of organic building blocks. The utility of DQ-SQ technique in determining the information about HB in various fluorine substituted molecules has been convincingly established.

Keywords: NMR spectroscopy; intramolecular hydrogen bond; organic fluorine

1. Introduction

1.1. Weak Molecular Interactions

The presence of molecular interactions in Nature cannot be ignored. The existence of various forms of matter, such as, solids and liquids is mainly due to the presence of intermolecular interactions. One can safely make a statement that the world would be a uniform ideal gas in the absence of intermolecular interactions.

The existence of intermolecular interactions is reflected at the molecular level, viz., the thermodynamic non-ideal-gas behavior arising due to vapor pressure, viscosity, virial coefficients, absorption, and superficial tension [1]. The molecular interactions are non-covalent and are inherently electrostatic in nature. These forces could be attractive, repulsive or the combination of attractive as well as repulsive between or within the molecules. They could also be between non-bonded atoms. Intermolecular interactions play predominant role in many fields, such as, conformation of biomolecules, drug design, etc.

Kaplan classified the intermolecular interactions on the basis of distance between the interacting objects [2]. In the classification, there are three main ranges for molecular forces depending on the

interatomic distances (*R*) for an interatomic potential (V). For range I the short distances are defined where the potential is repulsive in nature and the electronic exchange is due to the overlapped molecular electronic shells. The range II represents the intermediate distances with the van der Waals minimum, which arises due to the balance between repulsive and attractive forces. Range III represents the large distances with negligible electronic exchange where the intermolecular forces are predominantly attractive. The representation of range of molecular forces is illustrated in Figure 1a. Depending on the nature, the various molecular interactions can also be classified as given in the Figure 1b.

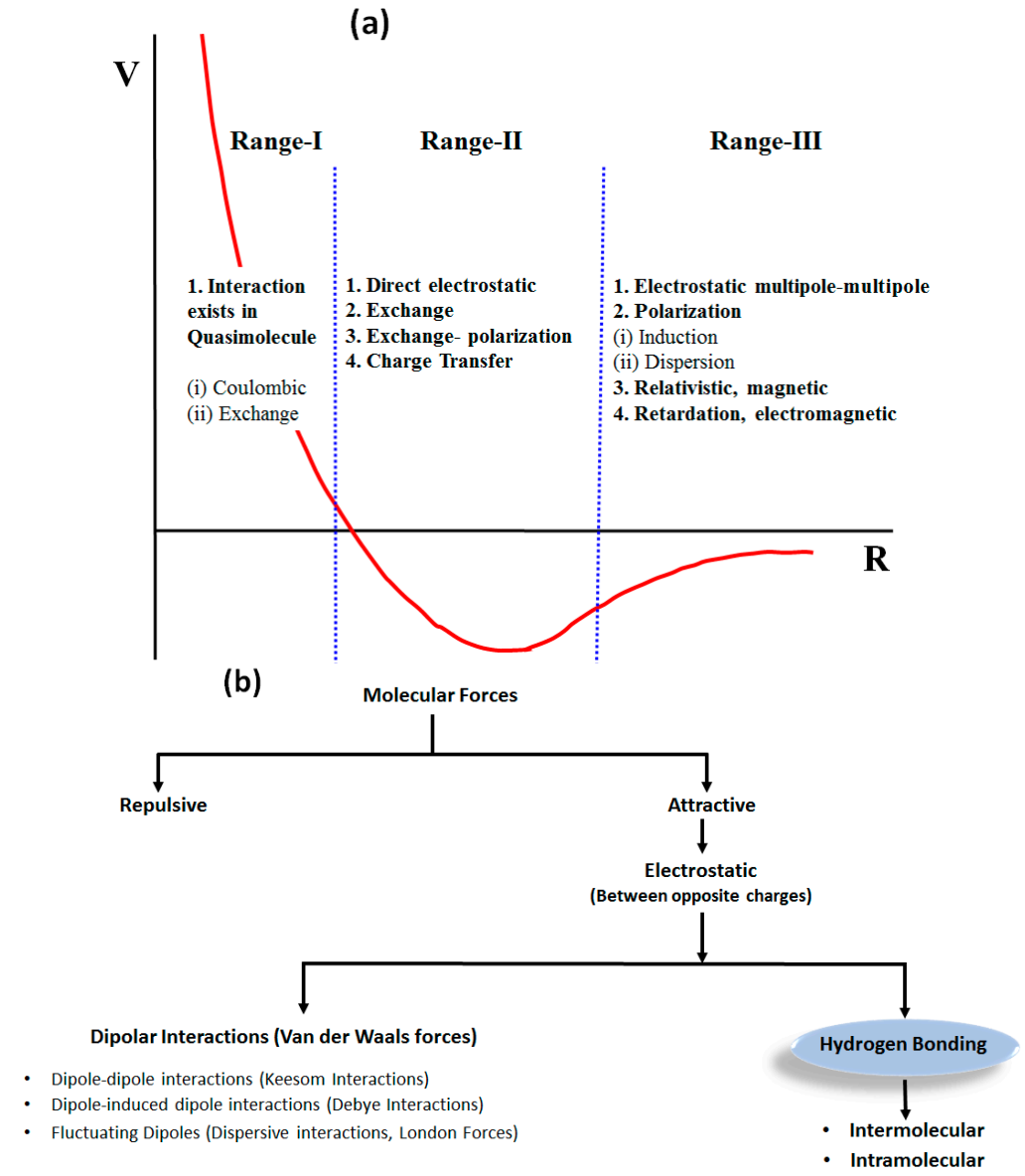

Figure 1. (**a**) The classification of intermolecular interactions on the basis of interatomic distances for a typical interatomic potential. Where *R* is the distance between the centers of masses of the molecules, V is the Lennard-Johns potential and the graph of V as the function of R is called Lennard-Johns model potential graph; (**b**) Schematic illustration of some of known molecular interactions. Some other molecular interactions that are not listed in the scheme may also be possible. This review is mainly focused on the intramolecular HB hence hydrogen bonding is highlighted in the scheme.

The change in molecular interactions are reflected in physical, chemical and biological phenomenon, such as, phase transitions of water (ice to water to vapor or vice versa), protein folding and unfolding and separation of DNA strands, RNA unfolding, etc. Such processes do not fall under chemical reactions. All the weak molecular interactions have their specific significance and govern the properties of a substrate it may be pointed out that the intermolecular interactions cannot be measured directly by any experiment.

Among all the weak molecular interactions described in Figure 1, except for the hydrogen bond (HB), usually pertain to intermolecular interactions. On the other hand, the HB can be detected within the molecule or between the two or more molecules. This review is focused on the studies carried out by authors' laboratory on the rare type of intramolecular hydrogen bonding (HB) involving organic fluorine.

1.2. Hydrogen Bond

The idea of HB was first suggested by Huggins [3–6] in 1919, and was further described by Larimer and Rodebush in 1920 [7]. HB is an interaction which occurs between an atom containing a lone pair of electrons (a Lewis base) and a hydrogen atom which is bonded to an electronegative atom (e.g., N, O, S or F) through a covalent bond. In a HB, the Lewis base plays the role of a HB acceptor (A) and the electronegative atom bonded to proton is called the HB donor (D). The hydrogen bonding interaction is schematically depicted in Figure 2.

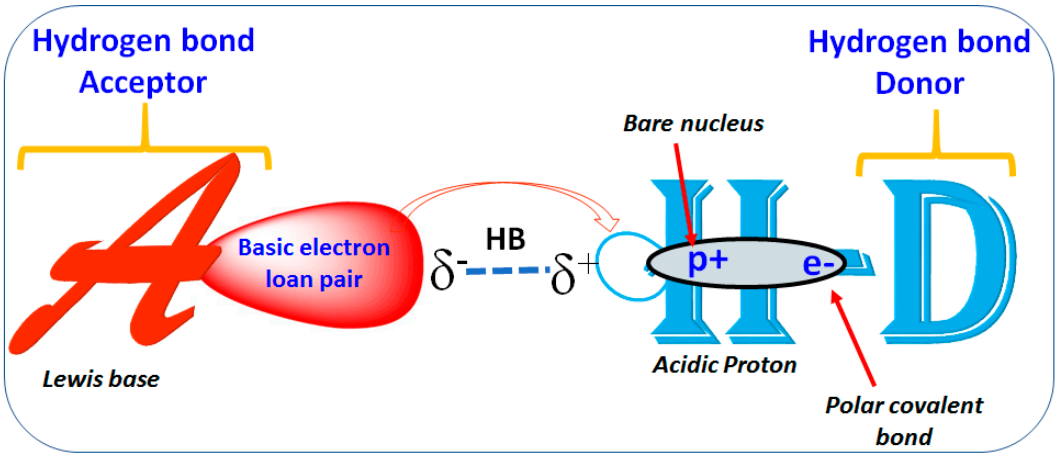

Figure 2. The pictorial illustration of hydrogen bond interaction, where HB acceptor/donor can be F, O, N, or S atom in the molecule. Polarization of electron and exposure of positive proton on either side is shown schematically.

Hydrogen is the only atom that easily participate in the HB. This is due to the fact that hydrogen atom can form covalent sigma bonds with electronegative atoms like F, N, O and S, etc., where the electron of 1s shells participates in the covalent bond. Since the more electronegative atom has tendency to pull the shared electron pair towards it, in the covalent bond between hydrogen and electronegative atom the bonding electrons moves away from hydrogen nucleus. Due to this the positive charge gets exposed from the back side (the opposite side to the bonded partner). This exposed positive nucleus attracts the partial negative charge of lone pair of the other nucleus. On the other hand, the atoms other than proton having non-bonding electrons in the inner shell shields the nucleus precluding it from getting exposed in this manner.

Importance of Hydrogen Bond

Hydrogen bonding is an important non-covalent interaction encountered most often in chemistry and biology [8–11]. Voluminous information is available on the self-assembly of molecules driven

by HB [12–24]. HB interaction is responsible for the three-dimensional conformation of proteins, synthetic foldamers [25–33], peptide catalysis, peptidomimetic design [34–39], double helical structure of DNA [40,41], unique properties of water [42], etc. Thus, in-depth knowledge of HB interaction aids in understanding the chemical properties of many organic and bio-macromolecules [43–53].

1.3. Organic Fluorine in the HB

A large fraction of the information available in the literature on intramolecular HB pertains to the motifs of the type O···H-N and N···H-N [54–58]. It is well known that organic fluorine hardly ever accepts HB. Dunitz and co-workers have even published a paper entitled "organic fluorine hardly ever accepts hydrogen bonds" [59–62]. Nevertheless, a few reports are available on the participation of organic fluorine in the HB in the solution state [63,64]. In foldamers and benzanilides, NMR and X-ray crystallographic studies have also been reported on the N-H···F-C HB [65,66]. Recently DFT theoretical studies have been carried out on organofluorine systems and through space J couplings have been also reported [67,68]. The first NMR spectroscopic observation of through space ($^{1h}J_{FH}$) coupling revealed the information about the involvement of organic fluorine in the HB in the solution state [69]. The Limbach group have reported numerous examples where not only organic fluorine but other halogens also participate in the intermolecular HB [70–73]. Subsequently this field of research has seen phenomenal growth. Furthermore, the utility of organofluorine molecules as drugs, agrochemicals, biomaterials and also in molecular imaging is well documented [74,75]. Organic fluorine also has enormous importance in molecular association applications, such as crystal engineering [76–78] and in the design of the functional materials [79]. Consequent to the binding nature of fluorinated molecules with enzyme active sites, intermolecular hydrogen bonds of the type X-H···F-C (X = O, N) are highly significant, especially in bio-inorganic and medicinal chemistry [80–84]. Despite all its importance in various branches of chemistry and biology, there is limited exploration of organic fluorine-involved HBs, attributed mainly to the fact flourine hardly ever accepts intramolecular HB [85–89]. The present review summarizes the work carried out by authors' laboratory in recent years, taken directly from their published work.

1.4. NMR Spectroscopic Techniques for the Detection of Hydrogen Bond

NMR spectroscopy has proven as a powerful tool in deriving information about HB. Monitoring of the chemical shift as a function of variation in the physical parameters, such as, dilution, temperature is a general technique adopted for gathering information about the HB. The other important parameter that can provide the unambiguous evidence about the existence of HB is through space coupling between two NMR active nuclei mediated by HB. Many of these parameters can be measured by various one and two dimensional NMR experiments.

1.5. Theoretical Calculations

The information derived by NMR spectroscopic analysis will conclusively evident if it is also corroborated by theoretical calculations. For such a purpose, various DFT-based theoretical calculations can be carried out. The commonly employed theoretical methods are briefly introduced below.

1.5.1. Non-Covalent Interaction (NCI) Calculations

For the detection of non-covalent interactions in real space, which is dependent on the electron density and its derivatives, NCI [90] calculations are performed. They provide a strong representation of the steric repulsion, van der Waals interactions and the HBs. The calculations yield a large positive gradient of the reduced density gradient (RDG), and the RDG values will be small and approach to zero in the density tail (i.e., regions far from the molecule, where the electron density exponentially decays to zero). This is the condition for both the covalent and non-covalent bonding regions respectively. There will be a strong correlation of electron density ($\rho_{(r)}$) with the weak interactions in the corresponding regions. The correlations for the HB are negative and positive for the steric effect. On the other hand,

for van der Waals interaction the $\rho_{(r)}$ values are always small [90] (near to zero). The calculated grid points are plotted for a defined real space function, $\text{sign}(\lambda_{2(r)})\rho_{(r)}$, as function 1 and reduced density gradient (RDG) as function 2.

1.5.2. Atoms in Molecules (AIM) Calculations

For in depth understanding of the molecular properties influenced by weak HBs the interaction energy must be known. The topology analysis technique has been reported and is cited as "atoms in molecules" (AIM) theory. It is also cited as "the quantum theory of atoms in molecules" (QTAIM) [91–95] which is dependent on the quantum observables (electron density $\rho_{(r)}$ and the energy densities). In topology analysis, the critical points (CPs) are those points where gradient norm of function value is zero (except at infinity). According to the negative eigenvalues of the Hessian matrix of the real space function [91–95] CPs can be of four types. Out of these the (3, −1) CP is called the bond critical point (BCP). The value of the real space function at the BCP has a great significance. For example, the bond strength and bond type respectively are related closely to the value of electron density ($\rho_{(r)}$) and the sign of Laplacian of electron density ($\nabla^2\rho_{(r)}$) at BCPs [91–95]. The sign of ($\nabla^2\rho_{(r)}$) at BCP is important in discriminating shared-shell (covalent bond (−ve)) and closed-shell (ionic, van der Waals interaction, and HB (+ve)). AIM calculations yield the magnitudes of $\rho_{(r)}$ and signs of $\nabla^2\rho_{(r)}$ for BCP of HBs of interest. At corresponding (3, −1) critical points (r_{cp}) the gradients of electron density ($\rho_{(r)}$) gets vanished. The energy of HB (E_{HB}) is directly related to potential energy density ($V_{(\mathbf{r})}$) by straightforward relationship $E_{HB} = V(r_{bcp})/2$ [96]. The E_{HB} of X···HX type HB can be calculated.

1.5.3. Natural Bond Orbitals (NBO)

Per-Olov Löwdin introduced the concept of *natural orbitals* in 1955, to describe the unique set of orthonormal 1-electron functions which are intrinsic to the *N*-electron wavefunction. NBO is calculated where the electron density could be the maximum. The general sequence of localized orbital is: (1) natural atomic orbitals (NAO); (2) natural hybrid orbitals (NHO); (3) natural bonding orbitals (NBO) and (4) natural (semi-) localized molecular orbitals (NLMO). These localized sets are considered as intermediate between basic atomic orbitals (AO) and molecular orbitals (MO). For the calculation of the electron density distribution in individual atoms and in bonds formed between atoms, NBOs are frequently utilized in computational chemistry. NBOs provide the percentage of highest possible electron density and most possibility for "natural Lewis structure" of ψ. During the formation of HB, the electron transfer from the HB acceptor (lone pairs (lp)) to the anti-bonding orbital (σ*) of the H atom takes place. NBO analysis is proved to be a powerful technique to obtain the detailed information of lp transfer.

1.5.4. Molecular Dynamics (MD)

The idea of molecular dynamics (MD) was first proposed in the 1950s [97]. MD is a computational method for studying the motion of atoms, groups, or molecules. MD studies give dynamic information about the atoms or group of atoms or molecules that interact for a period of time. During MD simulations, mostly the trajectories of atoms/molecules are stabilized where forces and potential energies among the particles are calculated by molecular mechanics force fields or interatomic potentials. MD is also called statistical mechanics by numbers and Laplace's vision of Newtonian mechanics of predicting the dynamics by animating nature's forces and revealing the information of molecular motion at an atomic scale. MD simulations are also found be very powerful in the detection and quantification of the percentage of different conformers of a molecule where there exists a freely rotating group.

2. Studies on Benzanilides

Isomers of fluorinated benzanilides belong to the class of molecules where the cooperative interplay of weak interactions is highly significant in building their higher analogues, called driven foldamers, supra-molecular clusters and bulk moieties such as dendrimers [86,98,99]. Hence these molecules have drawn great attention in structural chemistry. Furthermore, the C-F bond is longer, has opposite bond polarity, stronger than C-H bond and makes the molecule more resistant towards metabolic degradation. As a consequence, the families of these molecules have important biological applications as voltage dependent potassium channel openers [100–103]. Especially while modeling the higher analogs of benzanilides, three centered N-H···F HBs provide a new approach for the formation of structural features via strong binding effects and induced chirality upon complexation with chiral L-tyrosine-derived ammonium ions [86]. Hence extensive studies have been carried out on the intramolecular HB interactions in the fluorine-substituted derivatives of benzanilides [104].

2.1. NMR Spectroscopic Experimental Findings

NMR spectroscopy can be used to distinguish between labile free and hydrogen bonded protons, possessing different exchange rates, even in complex molecules if their exchange rates are within the NMR time scale [105–110]. Hence information about hydrogen bonding can be derived from the NMR spectral parameters [70,72,111–114]. Investigations have thus been carried out on a set of four derivatives of fluorinated benzanilides, whose chemical structures are reported in Figure 3, where there the fluorine substitution at positions X and/or $X^{/}$ has been systematically altered.

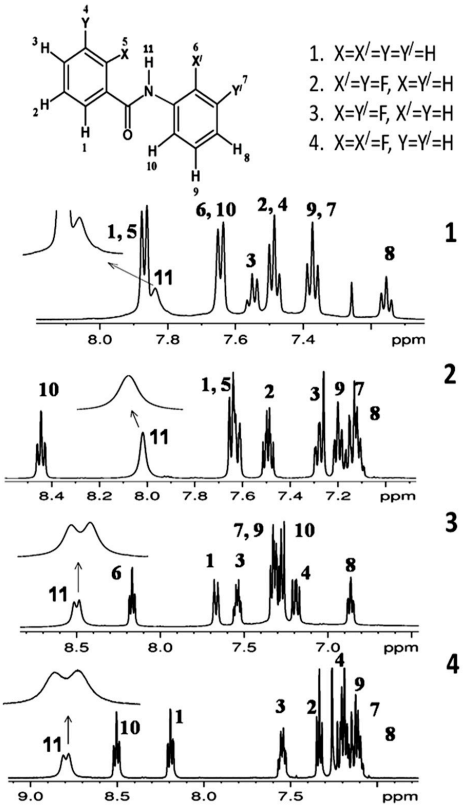

Figure 3. Chemical structures with numbering of interacting spins of fluorine-substituted benzanilides. The 400 MHz ^{1}H-NMR spectra of molecules **1**, **2**, **3** and **4** respectively (top trace to bottom trace) in the solvent $CDCl_3$. The peak assignments have been made based on multiple quantum (MQ)-single quantum (SQ) correlation experiments. The expansions for amide protons in each molecule are depicted by arrows (reproduced from [103]).

Unambiguous assignment of aromatic ^{1}H resonances have also been made employing the higher quantum correlation experiments for filtering of spectrum corresponding to different spin systems [115–117]. The systematic study by employing diverse one and two dimensional NMR experiments revealed information about the weak interactions in all the investigated fluorine-substituted derivatives of benzanilides at ambient conditions.

2.1.1. Detection of Spin-Spin Couplings Mediated by Hydrogen Bonds

NH proton signals are either singlets (in molecules **1**, **2**) or a partially resolved doublet (in molecules **3** and **4**). The peak separation of the partially resolved doublet is about 16 Hz. These partially resolved doublets might be due to the proton exchange between two distinguishable chemical environments or due to the existence of long range scalar couplings. The particular type of interaction responsible for this can be identified by either two-dimensional exchange spectroscopy (EXSY), or ^{1}H-{^{19}F} or ^{19}F-{^{1}H} experiments. The collapse of the NH doublets in both ^{1}H-{^{19}F} or ^{19}F-{^{1}H} spectra in the molecules **3** and **4**, is conclusively evident from Figure 4. This unambiguously established that the doublet detected for NH proton is due to the coupling between NH proton and ^{19}F. Such a large coupling value of NH proton is very unlikely for $^{5}J_{F(5)H(11)}$, $^{4}J_{F(6)H(11)}$, $^{5}J_{H(11)H(1)}$ and $^{4}J_{H(11)H(10)}$ [115–117] and has thus been attributed to the coupling between NH proton and ^{19}F atom mediated through hydrogen bond bridges between ^{19}F and ^{1}H.

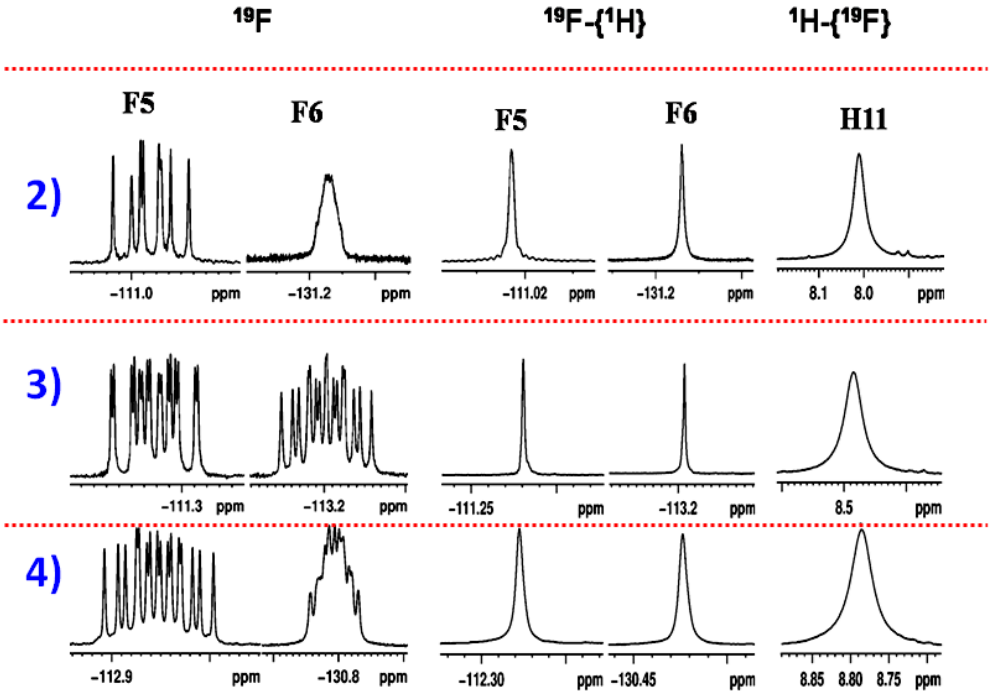

Figure 4. The 400 MHz ^{19}F, ^{19}F-{^{1}H} and ^{1}H-{^{19}F} NMR spectra of molecules **2**, **3** and **4** in $CDCl_3$.

2.1.2. Simultaneous Detection of Two through Space Couplings

In the molecules where X and X$^{/}$ are fluorine, the coupling of NH proton with both the fluorine atoms, even if it exists, could not be detected in the one dimensional ^{1}H spectrum. The excessively broad NH peak due to quadrupolar ^{14}N nucleus prevented the visualization of small couplings, if any. The ^{14}N decoupling achieved by systematic variation of the power and frequency of second irradiating RF over a wide range circumvented this problem of quadrupolar broadening and resulted in sharp NH signals as reported in Figure 5A.

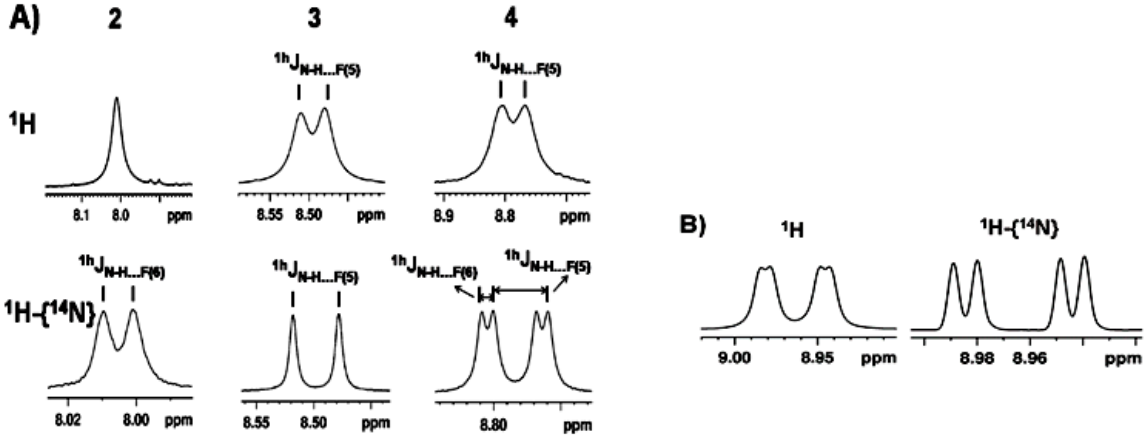

Figure 5. (**A**) The ^{1}H (left side) ^{1}H-{^{14}N} (right side) NMR spectrum of NH proton for the molecules **2**, **3** and **4** respectively at 298 K. (**B**) The ^{1}H and ^{1}H-{^{14}N} NMR spectrum of NH proton for molecule **4** at 230 K.

Nearly eight-fold reduction in line width of NH peak in **4** (reduced from 16 Hz to 2 Hz), resulted in a distinct doublet of doublet (dd) with measurable couplings of 17.7 Hz ($^{1h}J_{N\text{-}H\cdots F(X^{/})}$) and 3.7 Hz. Similarly, a doublet for molecules **3**, (16 Hz), and a doublet (3.6 Hz pertaining to $^{1h}J_{N\text{-}H\cdots F(X^{/})}$) for the NH proton of molecule **2** were detected at ambient temperature. Another interesting feature observed was the significant narrowing of NH signal on lowering the temperature (Figure 5B, molecule **4**). This is because of self-decoupling of NH proton with ^{14}N, at very low temperatures. However, this fact is not clearly obvious from the ^{1}H-{^{14}N} spectrum reported in Figure 5B as the decoupling at very low temperatures has very little effect on the line width due to the strengthening of the bifurcated HB at this temperature. Due to the slightly perturbed structural conformation, X$^{/}$(F) is not in close proximity with the amide proton. Thus in this case the hydrogen bond could not be detected by NMR as predicted by single crystal X-ray diffraction studies.

2.1.3. Temperature and Solvent Induced Perturbations

The investigated molecules were subjected to temperature variation over the range of 320–220 K in the $CDCl_3$ solvent. The chemical shift of NH protons (δ_{NH}) and $^{1h}J_{NH\cdots F}$ were monitored and their dependency on the temperature is plotted in Figure 6A for all the investigated molecules.

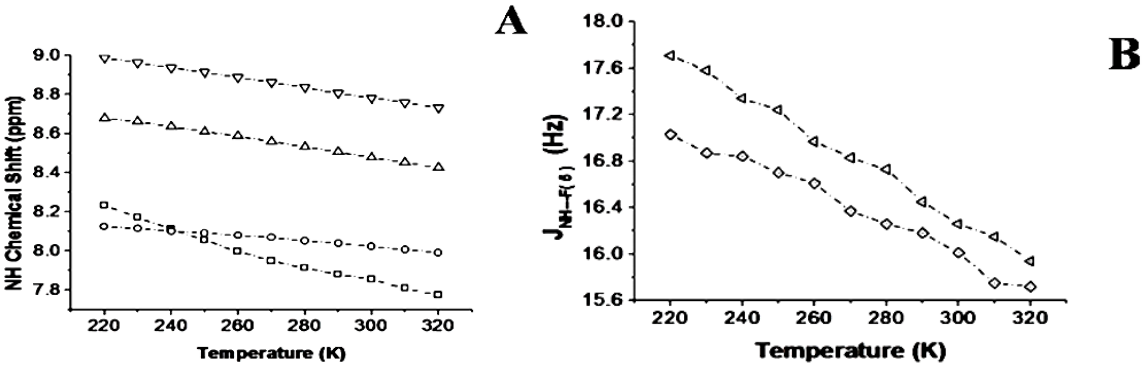

Figure 6. (**A**) Variation of chemical shift of NH protons (δ_{NH}) with temperature for all the investigated molecules. The squares, circles, upper triangles and inverted triangles correspond to molecules **1**, **2**, **3** and **4** respectively; (**B**) The variation of $^{1h}J_{N\text{-}H...F(5)}$, with temperature for molecules **3** and **4**. Squares pertain to molecules **3** and triangles correspond to molecule **4**.

HB gets strengthened on lowering the temperature and hence results in deshielding in the ^{1}H-NMR peaks as reported in Figure 6A. Another interesting observation is the change in $^{1h}J_{\text{N-H}\ldots\text{F(X)}}$. It varied from 17.03 (220 K) to 15.72 (320 K) Hz and 17.71 Hz (220 K) to 15.94 Hz (320 K) respectively for molecules **3** and **4**, as reported in Figure 6B, which provides clear and straightforward evidence in the favor of HB.

2.2. Theoretical Calculations

For the fluorinated oligomers ground state geometry optimizations, have been carried out. The geometry optimization was performed to enumerate the intramolecular N-H···F distances by employing the B3LYP/6-311+G** basis set [118]. Self-Consistent Isodensity Polarized Continuum Model (SCI-PCM) has been utilized to create the uniform $CHCl_3$ solvent environment [119]. Optimized molecular geometries along with HBs are reported in Figure 7.

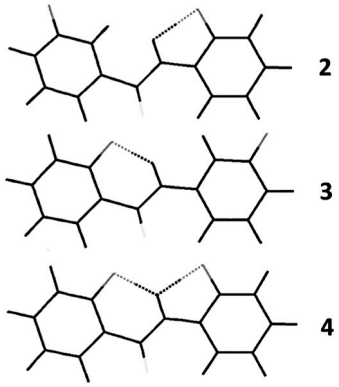

Figure 7. Optimized structures of fluorinated benzanilides visualized using Molden-4.7: HB parameters were measured by their optimization (Molden Control) in the vicinity of F···H-N HB distances and angles.

The theoretically observed HB distances involving N-H···F(X$^{/}$) are in close agreement with the X-ray structures [104].

3. CF_3 Substituted Benzanilides

Extending the study another series of CF_3 substituted benzanilides have been investigated [120]. The chemical structures of the investigated molecules are reported in Figure 8. In this series of molecules, the unambiguous evidence for the engagement of CF_3 group in N-H···F-C type HB, in the different CF_3 substituted derivatives has been observed in a low polarity solvent $CDCl_3$. It is well known that C(Sp^3)-F fluorine is a better acceptor than C(Sp^2)-F and C(Sp)-F fluorine [121]. To understand the role of CF_3 group in HB and in structural chemistry an extensive utility of NMR experimental techniques, including variable temperature and dilution studies, has been made. The first example of the engagement of the CF_3 group in the intramolecular HB of the type C-F···H-N has been reported [121–127]. The NMR findings have been additionally substantiated by molecular dynamics (MD) simulations.

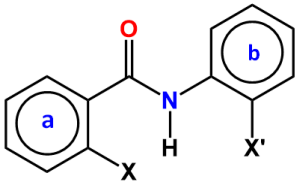

Molecules	X	X'
1	H	H
5	F	CF_3
6	H	CF_3
7	CF_3	CF_3
8	CF_3	H

Figure 8. Chemical structure of benzanilide (**1**) and its trifluoromethyl derivatives **5**–**8**.

3.1. NMR Experimental Findings

In the ^{1}H-NMR spectrum the NH proton of molecule **5** displayed a doublet with a separation of 16.7 Hz [120]. This is attributed to $^{1h}J_{FH}$ (coupling mediated through HB) between NH proton and the fluorine of ring a. Collapsing of this doublet to a singlet in the ^{1}H{^{19}F} experiment unambiguously established that it is mediated through HB, confirming the involvement of F in HB. Analogous to benzanilides discussed in the previous section, even in this molecule the excessive broadening of NH signal was observed, due to quadrupole relaxation by ^{14}N, may prevent the precise measurement of small couplings, if any, that may be hidden within the line width. In circumventing such problems, a 2D ^{15}N-^{1}H HSQC experiment has been carried out where ^{15}N is present in its natural abundance. The corresponding spectrum is reported in Figure 9.

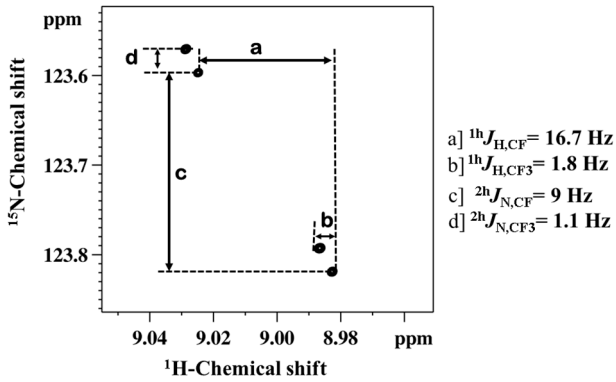

Figure 9. 400 MHz two-dimensional ^{15}N-^{1}H-HSQC spectrum of molecule **5** in the $CDCl_3$, depicting the through-space couplings. The measured coupling strengths are identified by a−d and their values have also been reported.

The two types of couplings mediated through HB, $^{1h}J_{FH}$ and $^{2h}J_{FN}$ are reflected in the ^{15}N-^{1}H-HSQC spectrum. The signs of couplings decided on the basis of the relative slopes of the displacement vectors assuming $^{1h}J_{FH}$ to be negative [104].

3.2. Theoretical Calculations

To ascertain the presence of weak molecular interactions established by NMR experiments in these molecules, the DFT based theoretical calculations have been carried out. Gaussian09 has been used at B3LYP/6-311+g (d,p) level of theory [118] for full-geometry optimizations of the molecules **5**–**8**. With the presence of three fluorine atoms in the CF_3 group there are various possible ways of interactions, such as, two centered, three-centered, or four-centered HBs. To derive the quantitative information about HBs, quantum chemical calculations and MD simulations have been carried out. For calculation, the geometry measurement criteria have been used in which HB is represented as N-H···F, where N is the donor atom and F is the acceptor atom. If the distance, r between N and F atom is less than 3.5 Å and the angle ∠NHF (θ) is greater than 120°, then an HB exists between the N and F atoms. The most probable distance, P(r), and appropriate angle, P(θ), are calculated for all the fluorine atoms in each of these four molecules. The percentage of occurrence of various types of HBs has been calculated from the MD simulations. A snapshot of the formation of HB and their percentage of the occurrence for the molecule **6** is reported in Figure 10.

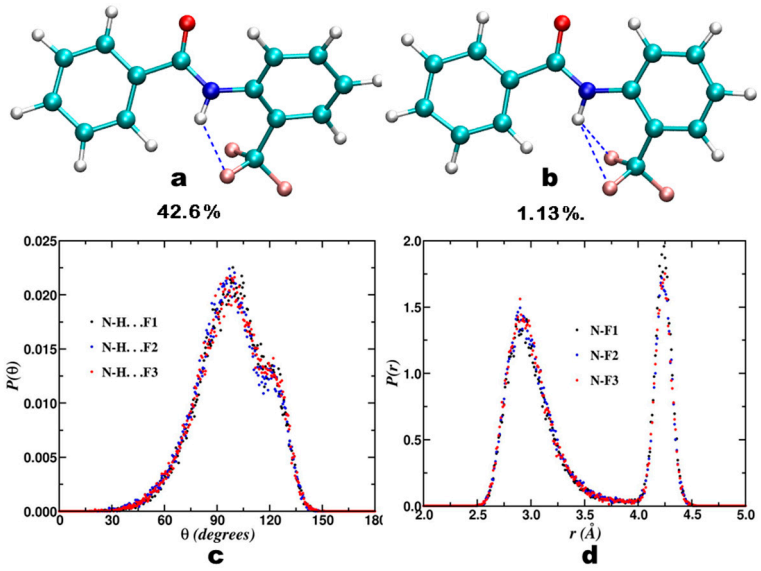

Figure 10. (**a**,**b**) Snapshot of HB formation in molecule **6**, along with their percentage of occurrence, obtained from MD simulations. Blue colored dashed lines show H-bonds; (**c**,**d**) Probability distributions of angles and distances, respectively.

The calculations reveal that the percentage of occurrence in a situation when there is no HB is 56.27%, whereas the occurrence of a two-centered HB is 42.60% (Figure 10a), and the occurrence of a bifurcated HB is much less and is 1.13% (Figure 10b). Figure 10c,d contain the HB geometrical parameters obtained by MD simulations. It has been observed that all the three F atoms in the CF_3 group have equal probability of forming HBs, as P(r) and P(θ) are same for three F atoms (Figure 10c,d).

For molecule **5**, where a single fluorine is substituted on ring "a" and the CF_3 group on the ring "b", there are five different possibilities of fluorine getting involved in the HB formation and also a possibility when there is no HB. All such possibilities with their percentage of occurrence determined by MD simulations are reported in Figure 11.

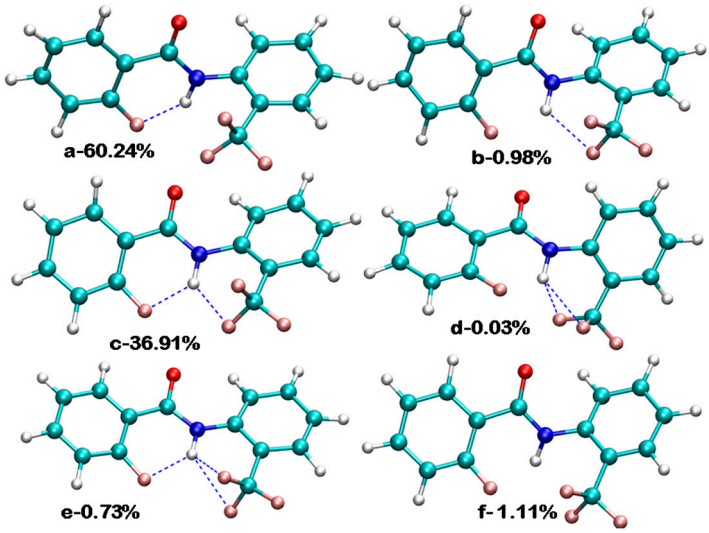

Figure 11. Various possibilities of HB formation for molecule **5**, with their % of occurrence obtained from the MD simulations (HB is shown by blue line).

A very interesting result has been derived from the $^{19}F\{^1H\}$ NMR spectrum of this molecule, which exhibited doublet and quartet patterns for CF_3 and CF groups, respectively. The corresponding

spectrum is reported in Figure 12. Fluorine atoms of CF and CF_3 groups in molecule **5** are separated by eight covalent bonds and the observed doublet peak with separation of 5.7 Hz is quite large. Thus the scalar couplings between the fluorine atoms, mediated through covalent bonds is quite unlikely. It can be safely attributed to the interaction between CF and CF_3 groups mediated through HB of the type F···H···F ($^{2h}J_{FF}$).

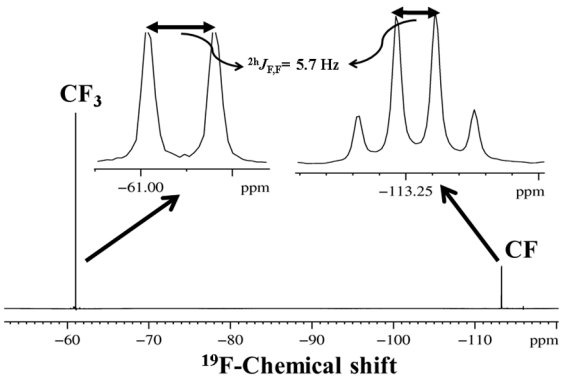

Figure 12. 376.7 MHz $^{19}F\{^1H\}$ NMR spectrum of molecule **5** showing $^{2h}J_{FF}$ through-space coupling.

The 2D-^{19}F-^{19}F COSY and *J*-resolved experiments also reflected the cross peaks pertaining to $^{2h}J_{FF}$ [120]. The strengths of HB for each fluorine atom present in all the molecules have also been calculated using atomistic molecular dynamics. The histogram of the HB formation H(r,θ) i.e., as a function of the distance, r between donor and acceptor atoms and θ the angle between donor-hydrogen-acceptor atoms, reported in Figure 13, have been calculated at 300 K for molecule **7**, from the 50 ns molecular dynamics simulation trajectory.

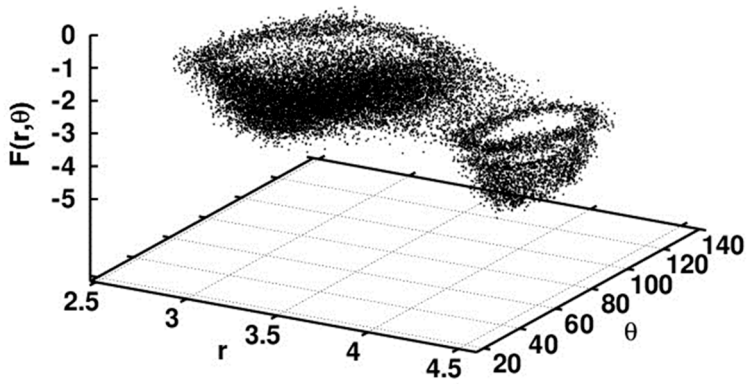

Figure 13. F(r,θ) for N-H···F1-C H-bond occurring in molecule **7**.

The free energy landscape of each atom involved in the HB calculation can be performed from this histogram using formulae given in the Equation (1):

$$F(r,\theta) = -k_B T \ln(2\pi r^2 \sin\theta H(r,\theta)) \quad (1)$$

For any fluorine atom participating in the HB with N atom, F(r,θ) has two minima corresponding to two states, one with HB and other with no HB. In the free energy landscape for molecule **7** given in Figure 13, for N-H···F_1-C the minima on the left-hand side is for HB (where r and θ satisfy the conditions for HB) and the other minima belongs to a situation where there is no HB. The strength of HB has also been calculated for the molecules **2**–**5** [120] using Equation (2):

$$E_{hb} = F^{hb}{}_{min}\,(r,\theta) - F^{no-hb}{}_{max}\,(r,\theta) \quad (2)$$

where $F^{hb}{}_{min}$ (r, θ) is the minima of hydrogen bonded state and $F^{no-hb}{}_{max}$ (r, θ) is the maxima for no hydrogen bonded state.

4. Studies on Hydrazides

Hydrazides are organic compounds that share a common functional group with a N-N covalent bond where at least one of the four substituents should be an acyl group [128]. Different derivatives of hydrazides have proven to be extremely important as, reagents in organic synthesis [129], anti-tumor medicine [130,131], and also in the cytotoxic functioning [132]. In combination with other cmedicines, the derivatives of hydrazides are utilized for the treatment or prevention of tuberculosis [133].

4.1. N,N-Diacyl Substituted Derivatives of Hydrazides

The hydrazides provide a possibility to synthesize a variety of derivatives with different combinations of substituted acyl group(s) of interest. The different derivatives of hydrazides have been synthesized and characterized using one and two dimensional multinuclear NMR experiments, and ESI mass spectrometry. The procedure for synthesis of these molecules and the NMR spectral analysis have been reported [134]. The NMR experiments reveal the existence of weak intramolecular interactions in all the investigated derivatives of hydrazides [134]. The NMR derived HB information has been further ascertained by DFT [135,136] based NCI [90], and QTAIM [91–95] calculations.

4.1.1. NMR Spectroscopic Detection

One of the NMR spectral parameters that provides information on the HB is the variation of chemical shift under different experimental conditions. In the reported work [134] the different derivatives of hydrazide, **9**–**18**, generically named 2-X-*N*-(2-X′)benzohydrazides, whose basic chemical structures and their site specific substituents, reported in Figure 14, have been investigated. The disubstituted molecules are classified into two categories, one where X = X′ (**9**–**11** and **18**) and the other where X ≠ X′ (**12**–**17**).

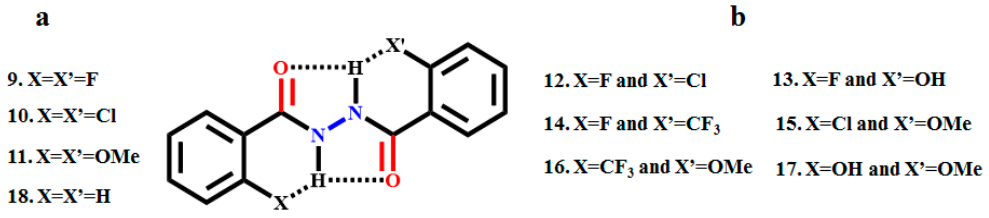

Figure 14. The chemical structures of 2-X-*N*-(2-X′) benzohydrazide derivatives; (**a**) symmetrically substituted molecules and (**b**) asymmetrically substituted molecules.

For discarding any possibility of dimerization or self-aggregation, if any, 2D DOSY [137,138] experiments, ESI-MS analysis and dilution studies have been carried out. Solvent titration experiment [63,64,139] has been employed to understand the weak interactions, such as, intra- and inter- molecular HB, to compare their relative strengths of interaction and also to evaluate the effect of monomeric water on HB, which is absorbed from the atmosphere. The variation in the chemical shift of NH proton as a function of temperature (300–220 K) is compared for all the investigated molecules in Figure 15b. On lowering the temperature, the NH peak of all investigated molecules except one NH proton peak of molecule **13** is showed downfield shift due to the strengthening of HB. The unusual behaviour of this NH proton of the molecule **13** has been attributed to the switching of this molecule to another possible conformer on lowering the temperature. The possibility of such a switching phenomenon is illustrated in Scheme 1.

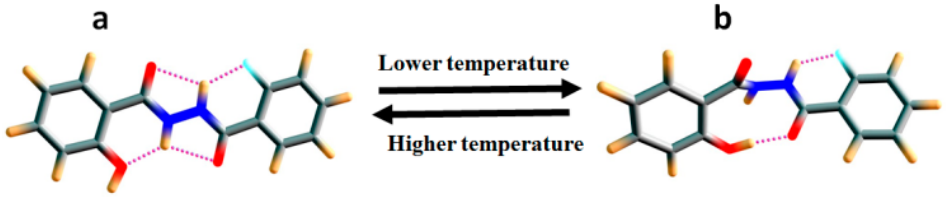

Scheme 1. Two different possible stable conformations of molecule **13**, (**a**) at higher temperature; and (**b**) at lower temperature.

The relative strength of intramolecular HBs has been qualitatively derived by titration with dimethylsulphoxide (DMSO) solvent [134]. The observed variation in the chemical shifts as a function of the incremental addition of DMSO-d_6 is plotted for the molecules **9**–**17**, in Figure 15c. Disruption of intramolecular HB [104] by the solvent DMSO results in the deshielding of NH protons. On the contrary for the NH protons of molecule **11**, and one of the two NH protons of asymmetric molecules, **15**–**17** the high field shift was detected on addition of DMSO-d_6. This is due to the fact that these NH protons involved in HB with OMe group are relatively stronger than the DMSO interaction. The high field shift of these protons is attributed to an equilibrium which is stabilized between intra- and inter- molecular hydrogen bonded species.

Another strong evidence in the favour of organic fluorine involved intramolecular HB is the detection of through space couplings between the NH proton and fluorine [40,140–142]. The ^{19}F coupled and decoupled ^{1}H spectrum of molecule **9** in the solvent $CDCl_3$, and the ^{19}F coupled spectrum in the solvent DMSO-d_6 are given in Figure 16. The NH peak of the molecule **9** is a doublet with a separation of 12.75 Hz (Figure 16a). This doublet collapsed into a singlet in the ^{1}H{^{19}F) experiment confirming the presence of the coupling between ^{1}H and ^{19}F (Figure 16c). The doublet also collapsed to a singlet in a high polarity solvent DMSO-d_6 (Figure 16b).

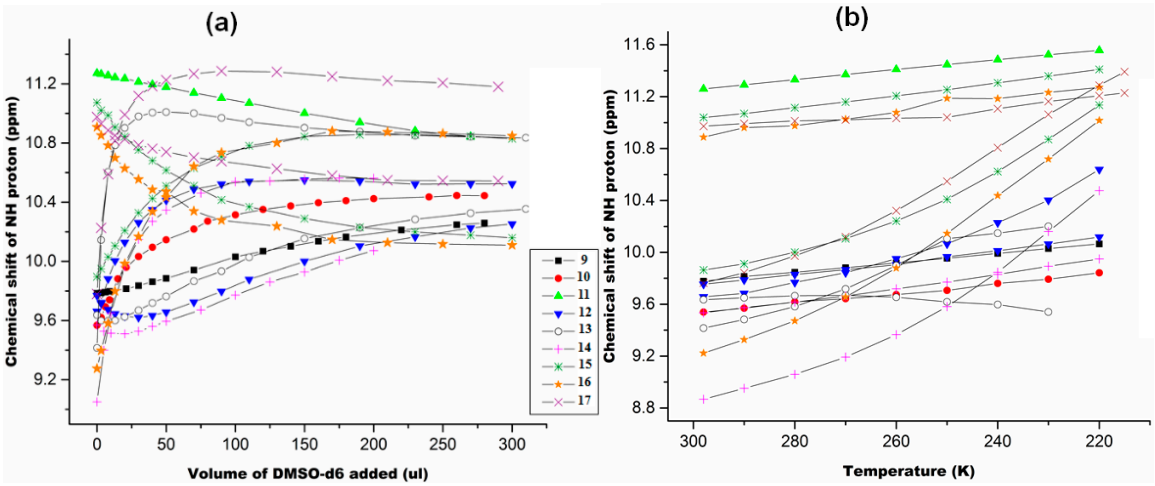

Figure 15. (**a**, **b**) Variation in the chemical shifts of NH proton as a function of temperature and the volume of DMSO-d_6 respectively for the molecules **9**–**17**. The initial concentration was 10 mM in the solvent $CDCl_3$. (**a**) The DMSO-d_6 was incrementally added to an initial volume of 450 µL in $CDCl_3$, at 298 K; (**b**) The temperature was varied from 300 to 220 K. The molecules **9**–**17** are identified by the symbols given in the inset.

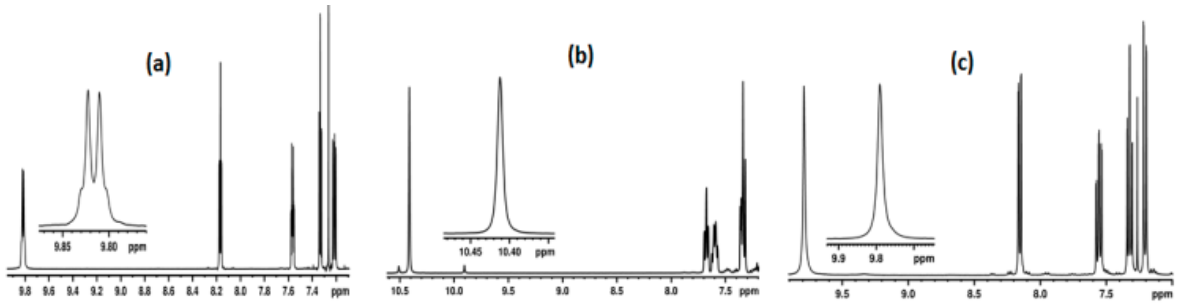

Figure 16. 400 MHz ^{1}H-NMR spectrum of molecule **9**, (**a**) in $CDCl_3$; (**b**) ^{1}H-NMR spectrum in DMSO-d_6 and (**c**) $^{1}H\{^{19}F\}$ NMR spectrum in $CDCl_3$.

The $^{3}J_{HH}$ and $^{4h}J_{FH}$ couplings, if any, are not detectable due to the symmetry of the molecule. For detection of these couplings the symmetry of the molecule has to be broken. For such a purpose 2D ^{1}H-^{15}N HSQC experiment has been carried out for the molecule **9**, where ^{15}N is present in its natural abundance. The HSQC spectrum is reported Figure 17A where all the possible seven couplings, $^{1}J_{NH}$, $^{2h}J_{FN}$, $^{2}J_{NH}$, $^{3h}J_{FN}$, $^{1h}J_{FH}$, $^{4h}J_{FH}$ and $^{3}J_{HH}$ has been measured from this spectrum. The observation of through space couplings of significant strengths, such as $^{1h}J_{FH}$, $^{2h}J_{FN}$ $^{3h}J_{FN}$ and $^{4h}J_{FH}$, provided strong and direct evidence for the involvement of organic fluorine in the intramolecular HB. In the solvent DMSO, except for $^{1}J_{NH}$, all the other couplings mediated through HB disappeared as reported in Figure 17B.

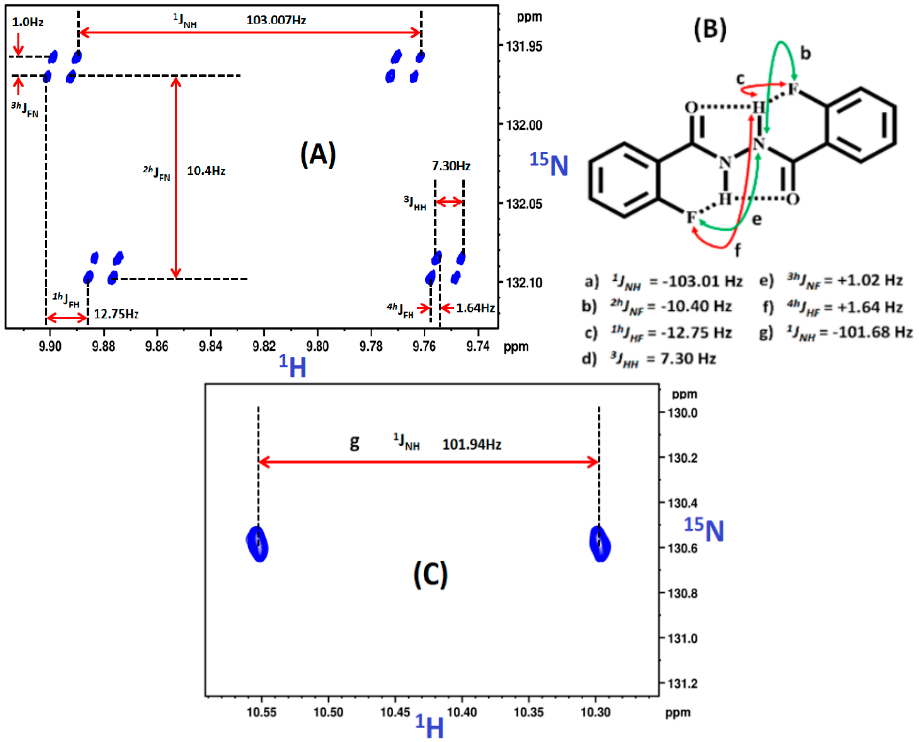

Figure 17. (**A**) 800 MHz ^{1}H-^{15}N-HSQC (NH-coupled) spectrum of molecule **9** in $CDCl_3$; (**B**) the chemical structure of the molecule **9** with marking of couplings determined and their magnitudes; (**C**) 400 MHz ^{1}H-^{15}N-HSQC spectrum (NH-coupled) in DMSO-d_6.

The relative signs of all the couplings were determined with respect to coupling c marked in Figure 17B. From this it was inferred that $^{1h}J_{FH}$ is negative. The comparison of $^{1}J_{NH}$ [143,144] of molecules **9**–**17** with unsubstituted molecule **18**, provided ample evidence that the nature of HBs in

derivatives of hydrazides are predominantly covalent in nature. The close proximity of NH proton with the fluorine in fluorinated molecules is detected by 2D HOESY (hetero-nuclear Overhauser effect spectroscopy) experiment. This also provided evidence in favor of intramolecular HB.

4.1.2. NCI Plot

The weak molecular interactions established by NMR studies have also been corroborated by theoretical DFT [135,136] optimized structure based calculations. The calculation of noncovalent interaction (NCI) has been shown to be very useful technique for the visualization of weak interactions [90]. The calculated grid points are plotted for a defined real space function, sign($\lambda_{2(r)}$)$\rho_{(r)}$, as function 1 and reduced density gradient (RDG) as function 2 and also the color filed isosurfaces for all the investigated molecules. Figure 18 gives these plots for the molecule **9**.

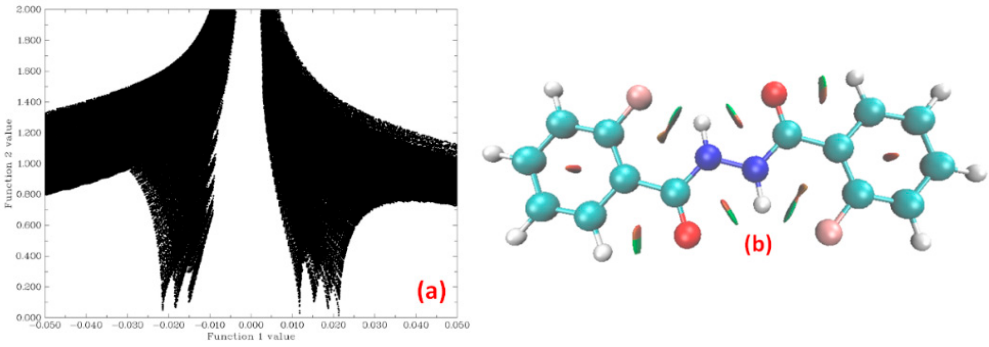

Figure 18. (**a**) The plot of sign($\lambda_{2(r)}$)*$\rho_{(r)}$ as function 1 v/s the RDG as function 2; and (**b**) coloured isosurface plot (green color denotes weak H-bond and red color stands for steric effect) for molecule **9**.

There are three spikes on the left hand side of Figure 18a (i.e., sign($\lambda_{2(r)}$)*$\rho_{(r)}$ is negative) denoting three HBs, viz., N-H···F, N-H···O and C-H···O. These three HBs can be observed in Figure 18b as green coloured isosurfaces. The red colour in isosurface plot (Figure 18b) represents the steric hindrance arising from phenyl ring of the molecule and other HB mediated rings. This is seen as four spikes on the right hand side (i.e., sign($\lambda_{2(r)}$)*$\rho_{(r)}$ is positive) of Figure 18a. Similar results have been derived for all other investigated molecules [134].

4.1.3. Atoms in Molecules (AIM) Calculations

The magnitudes of $\rho_{(r)}$, signs of $\nabla^2\rho_{(r)}$ and potential energy density ($V_{(r)}$) at corresponding (3, −1) BCP (bond critical points) (r_{cp}) for HBs of interest have been calculated using QTAIM calculations [91–95]. The value of ($V_{(r)}$) used in the $E_{HB} = V(r_{bcp})/2$ [96] for the calculation of energy of HB (E_{HB}) of X···HX type. The calculated E_{HB} of different HBs in all investigated molecules ranged between −3 to −8.6 Kcal/mol [134].

The ^{1}H-NMR spectra were simulated using the GIAO [145] and CSGT [145] methods. It is observed that in most of the cases there are more than one conformers for the molecules. Thus the calculated chemical shift values of NH protons are not in complete agreement with the experimental data. The values observed from CSGT method are comparable with the experimental results.

4.2. N, N Acyl-Phenyl Substituted Derivatives of Hydrazides

In this work another series of hydrazide derivatives has also been synthesized and investigated, where the formation of five and six membered rings mediated through HBs is possible. The general chemical structure is given in the Figure 19.

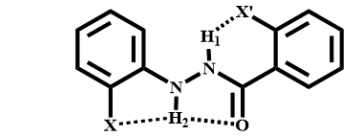

19. X=X'=H **21.** X=H and X'=F **24.** X=F and X'=OMe
20. X=X'=F **22.** X=F and X'=H **25.** X=CF_3 and X'=OMe
23. X=CF_3 and X'=H

Figure 19. The chemical structures of *N′*-phenylbenzohydrazide and its halo derivatives. The dotted lines indicate the HB.

The main focus of this work is to determine the conformations of the fluorinated hydrazide derivatives and thereby understanding the effect of HB of the type F/CF_3···H (N).

4.2.1. Spectroscopic Experimental Observations

For initiating the study, the ^{1}H-^{19}F HOESY experiments have been carried out for all the investigated molecules and the strong correlation in ^{1}H-^{19}F HOESY spectrum is observed where fluorine (X′) in the phenyl ring B established correlation with $NH_{(1)}$ proton whereas fluorine in the phenyl ring A (X) established correlation with $NH_{(2)}$ proton. From the obtained correlations, the conformations of all the synthesized molecules have been derived and ^{1}H-^{19}F HOESY spectrum for the molecule **20** is reported in Figure 20.

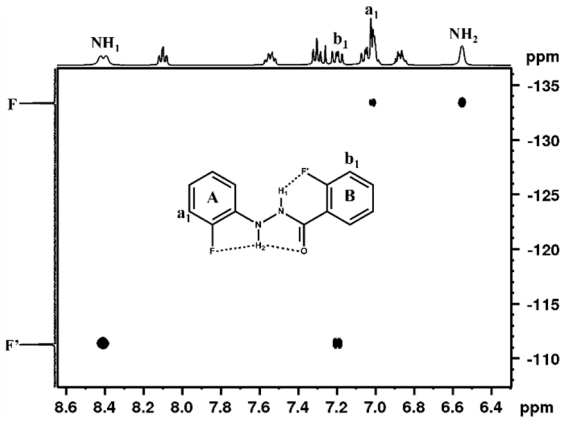

Figure 20. 400 MHz two dimensional ^{1}H-^{19}F HOESY spectrum of molecule **20**. The detection of strong cross peaks convincingly established the correlations between $NH_{(1)}$ proton and F and also $NH_{(2)}$ proton and F. The cross peaks were also observed for phenyl protons a_1 and b_1. The mixing time used in the experiment was 450 ms.

After arriving at the conformations of the molecules, the further studies were directed to derive the information about the weak molecular interactions (HB) that validate the proposed conformations. The titration experiment with $CDCl_3$ did not show any significant change in the chemical shift of NH protons confirming the absence of any intermolecular interactions. The peak at 1.54 ppm corresponding to monomeric water remain constant indicating the absence of hydrizide-water interaction [146]. For discarding the possibility of dimerization or aggregation, if any, DOSY experiment has been carried out with the mixture of 1:1 molar ratio of molecules **20** and **25** in the solvent $CDCl_3$, which have different diffusion coefficients.

The ^{1}H-NMR spectra for the investigated molecules have been acquired at different temperatures where the HB gets strengthened on lowering of temperature and results in deshielding of the NH proton participating in HB. The corresponding plots of temperature dependent variation of chemical

shifts of NH protons are reported in the Figure 21A,B. In addition to this the incremental additions of DMSO-d_6 resulted in the deshielding of NH proton providing information about the strength of HB. The perturbation on the chemical shifts of NH proton (δ_{NH}) induced by DMSO-d_6 are given in Figure 21C,D. The temperature coefficient is directly proportional to the strength of HB. On the other hand, the $\Delta\delta_{NH}/\Delta V_{DMSO}$ has inverse relation to the strength of HB. Hence mere visual inspection of the graphs given in Figure 21 provides information about the comparative strengths of HB in the studied molecules.

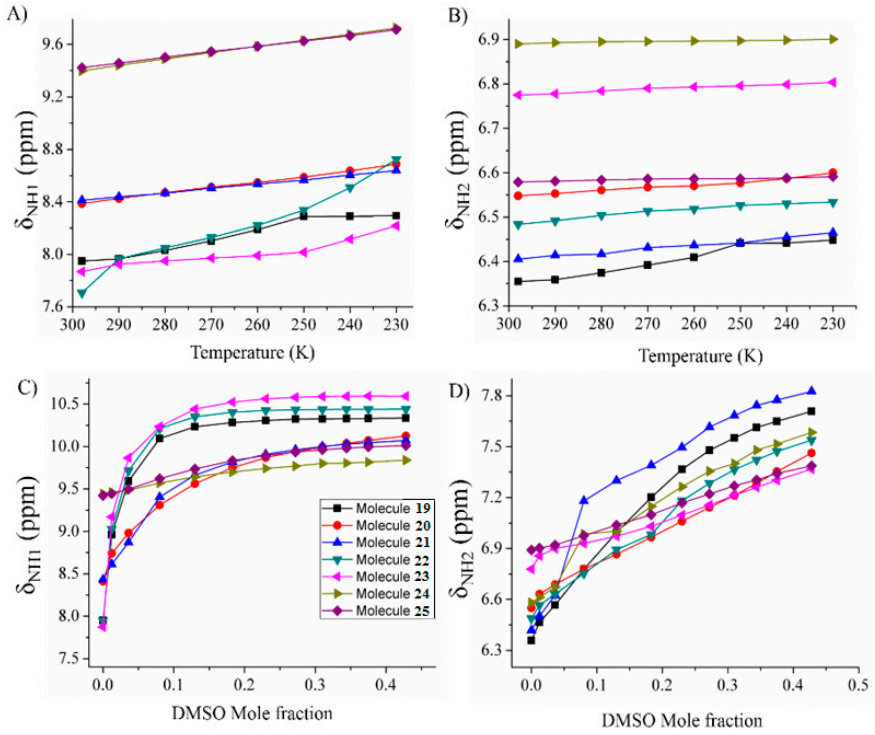

Figure 21. The variation of the chemical shift of; (**A**) $NH_{(1)}$; (**B**) $NH_{(2)}$ protons with temperature; (**C**) $NH_{(1)}$ and (**D**) $NH_{(2)}$ protons with the incremental addition of DMSO-d_6 for the molecules **19**–**25** in the solvent $CDCl_3$ at 298 K. The color code for the molecules are given as an inset in Figure 21C, and is same for Figure 21A–D.

The direct evidence about the presence of HB can be obtained by deriving the coupling between two NMR active nuclei which are participating in the formation of HB. In order to overcome the broadening (due to quadrupolar ^{14}N nucleus) in the NMR spectrum, the 2D ^{15}N-^{1}H HSQC spectra have been recorded for all the investigated molecules where ^{15}N is in natural abundance. The expanded $NH_{(2)}$ region of ^{15}N-^{1}H HSQC spectrum of molecule **20** in $CDCl_3$ is given in Figure 22 which provides values of $^{1h}J_{FH}$ and $^{2h}J_{NF}$. These $^{1h}J_{FH}$ and $^{2h}J_{NF}$ detected in the solvent $CDCl_3$, disappeared in the solvent DMSO-d_6. This unequivocally established that these are coupling arising from through space interactions.

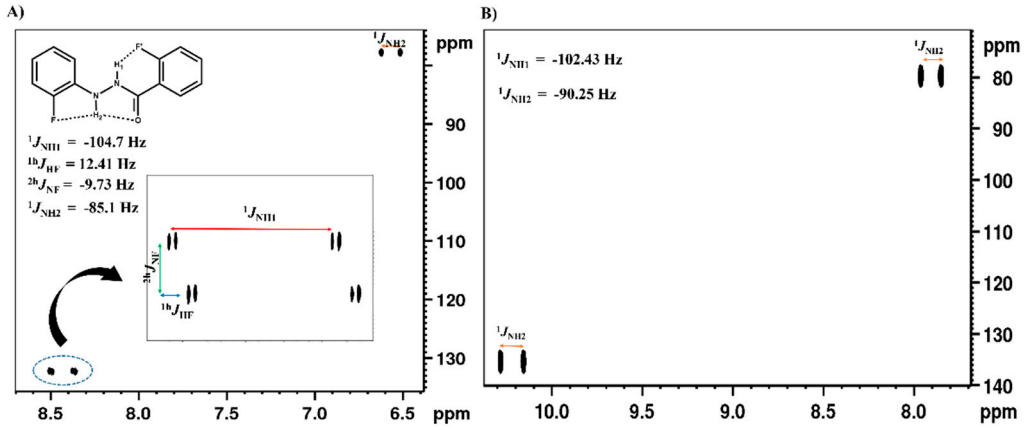

Figure 22. 400 MHz coupled ^{15}N-^{1}H-HSQC spectra of molecule **20** in the solvents (**A**) $CDCl_3$ and (**B**) DMSO-d_6. The measured couplings and their signs are reported in the Figure 22A.

Furthermore, in the 2D ^{15}N-^{1}H HSQC spectrum of molecule **25**, the $NH_{(2)}$ peak appeared as a quartet in $CDCl_3$ while it appeared as a singlet in DMSO solvent indicating that the couplings observed in $CDCl_3$ are the through space contribution [134]. The $^1J_{NH}$ scalar coupling is another important NMR parameter for extracting the information about the nature of HB [40,144,147]. There is a significant increase in $^1J_{NH(1)}$ and $^1J_{NH(2)}$ values in halo/methoxy substituted molecules compared to the unsubstituted molecule of hydrazide, confirming that the corresponding HBs are predominantly electrostatic in nature.

4.2.2. Theoretical Calculations

The observed NMR experimental results have been corroborated by IR and QTAIM [91–95], NCI [90] and the conformational study by using relaxed potential energy scan. The chemical structures of all the synthesized molecules have been optimized using G09 program with B3LYP/6-311G** level of theory by taking chloroform as a solvation medium. The molecular structures were also optimized with larger basis set like aug-cc-pVTZ and ^{1}H-NMR spectra were simulated using GIAO [145] method for optimized structures (both by 6-311G** and aug-cc-pVTZ basis sets) in chloroform solvation medium.

Additional information has been derived by IR and QTAIM an NCI analysis. The C=O and N-H stretching frequencies in the IR spectra of all the investigated molecules showed blue shift, providing an evidence for the existence of HB [148]. Positive sign for Laplacian of electron density ($\nabla^2\rho$) at the $NH_{(1)}\cdots X'$ [148] indicates that in all the molecules the type of interaction is HB.

The NCI index detects the weak interactions in real space based on the electron density and its derivatives. Using Multiwfn program, the grid points have been calculated and plotted for the two functions: sign(λ2)*ρ as function 1, and reduced density gradient (RDG) as function 2. Both these functions have the information about HB. The color filled isosurface graphs show the presence of H(N)···X–C and C=O···H(N)···X–C type HBs in the investigated molecules. These calculations further supported the NMR observations.

Relaxed Potential Energy Scan

In NMR study, the $NH_{(2)}$ proton of molecule **25** appeared as a quartet in ^{1}H-^{15}N HSQC spectrum. To understand the reason behind the observation of quartet the relaxed potential energy scan has been performed using B3LYP/6-311G** level of theory at ambient temperature for the F28–C27–C5–H12 dihedral angle through which the internal rotation of the CF_3 group was confirmed (Figure 23). The calculated energy barrier for the CF_3 internal rotation is about 2.31 kcal/mol. Because of such a low energy barrier CF_3 group appeared as a quartet in NMR spectrum.

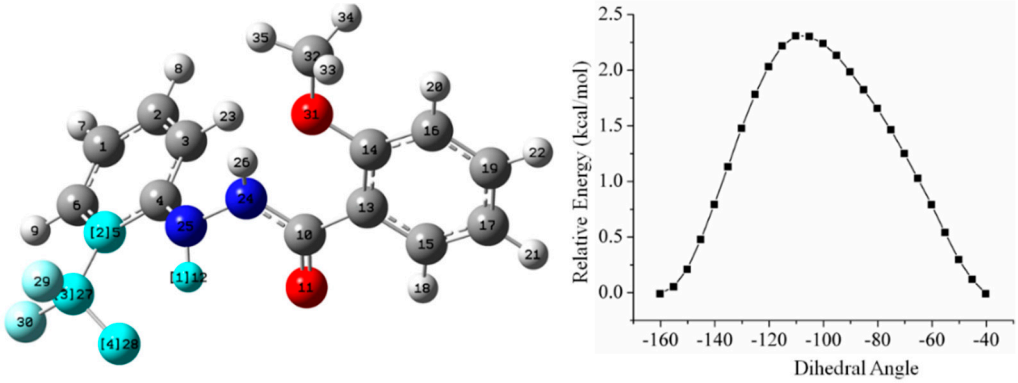

Figure 23. Relaxed potential energy surface Scan for the internal rotation of the CF_3 group. The scan was performed in 28 steps with increments of 5° in the dihedral angle.

The relaxed potential energy surface scan has also been carried out for the molecule **20** using B3LYP/6-311G** level of theory at ambient temperature in 36 steps with 10° increment in the dihedral angle (−180° to +180°) in order to get the information about the internal rotation of the phenyl ring through a single bond. From Figure 24 it is clear that the proposed conformation has lower energy over the other.

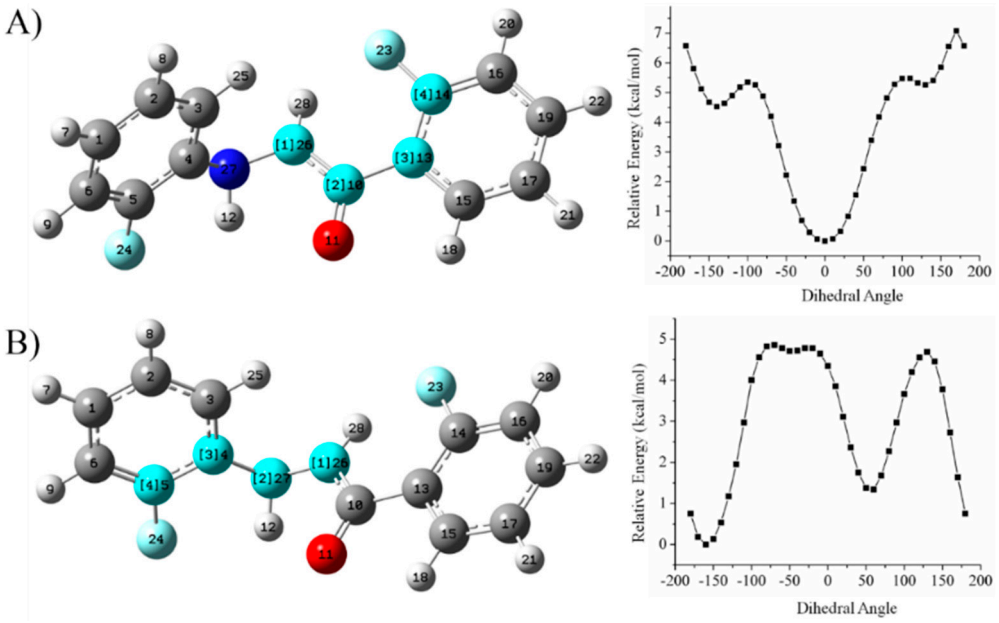

Figure 24. Relaxed potential energy surface scan for the internal rotation of phenyl ring through a single bond in molecule **20**. Selected dihedral angles; (**A**) N26–C10–C13–H14 (**B**) N26–N27–C4–C5.

5. Studies on Derivatives of Imides

The imides are the diacyl derivatives of ammonia or the primary amines [128]. The importance of imide derivatives is found in many field of daily interest such as, high strength electrically conductive polymers [149–151], synthetic applications [152], medicinal activity [153], as ionic fluids [154], in pharmacology [155] and as synthetic precursors [156] are well documented. The NH linker of an imide provides ample scope to synthesize different derivatives with the desired substitution on acyl group(s). Several derivatives of imides whose chemical structures are given in the Figure 25 have been synthesized by using microwave assisted method [157] and characterized by extensive utility of NMR techniques and ESI-HRMS spectrometry [158].

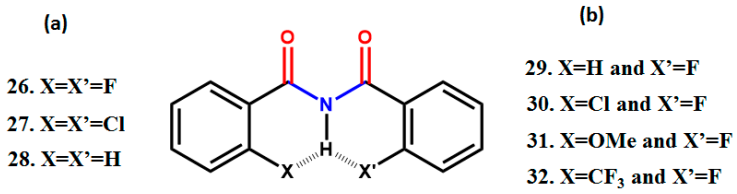

Figure 25. The chemical structures of the derivatives of 2-*X*-*N*-(2-*X*′-benzoyl)benzamide.

5.1. Information Derived by NMR Spectroscopy

The NMR spectroscopic derived information on intramolecular HB in these molecules has been unequivocally supported by Density Function Theory DFT [135,136] based NCI [90,159], and QTAIM [91–95] calculations.

The solvent titration experiments [62,63,140] have been performed on the molecules **26**–**32** in the solvent $CDCl_3$ to distinguish the intra- and inter- molecular HB and to monitor the effect of atmospheric monomeric water on HB. It is observed that there is no change in the chemical shift of NH proton as well as the residual water peak position in the deuterated solvent [158]. These observations discarded any possibility of intermolecular HB, aggregation, dimerization or water-imide interaction.

DMSO-d_6 solvent titration has been employed to derive the qualitative information on the relative strengths of intramolecular HB on the molecules **26**–**32**. The excessive deshielding of NH proton is observed as a consequence of the disruption of intramolecular HB due to the strong interaction with DMSO. The upfield shift for NH peak with the addition of DMSO [158] in the molecule **6**, indicated that in this particular molecule, the intramolecular HB formed between oxygen atom of the methoxy group and NH proton might to be stronger than its interaction with DMSO [134]. The strength of HB gets increased on lowering the temperature. Excessive deshielding of the NH proton is observed on lowering the temperature due to the displacement of hydrogen bonded proton towards the HB acceptor. This is an evidence in favor of intramolecular HB [160–162]. The chemical shift of NH protons as a function of temperature (over the range of 298–220 K) for molecules **26**–**32** are contained in Figure 26A.

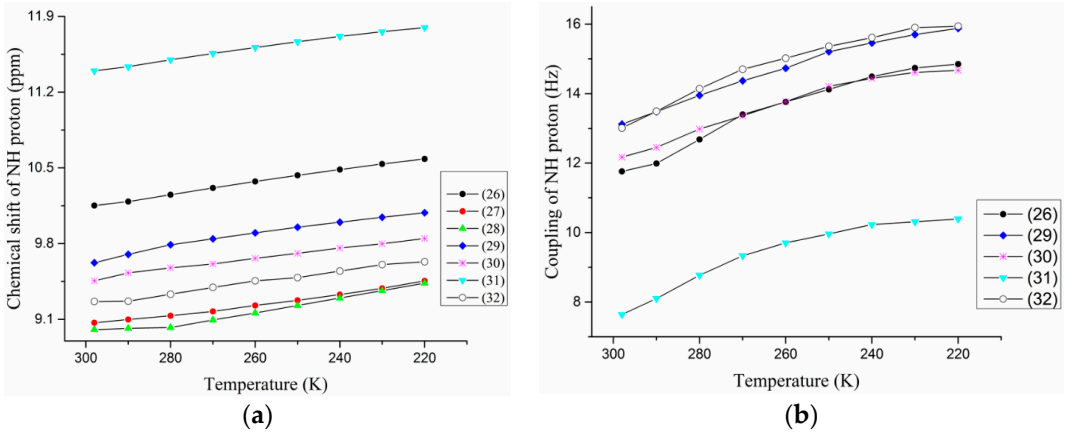

Figure 26. Variation of (**a**) chemical shifts of NH protons as a function of temperature for the molecules **26**–**32** and (**b**) through space mediated HF coupling constant as a function of temperature for the molecules **26** and **29**–**32**. The molecules are identified by the symbols given in the inset. The initial concentration was 10 mM in $CDCl_3$.

The change in FH coupling value on lowering the temperature has also been detected. Such a variation is possible only when the spin polarization is transmitted between two NMR active nuclei mediated through HB. The variation in the coupling constant (through space) as a function of temperature is reported in the Figure 26B, for the molecules **26** and **29**–**32**.

The GIAO [145] and CSGT [145], DFT methods of NMR simulation have been used for chemical shifts calculation and it has been observed that the CSGT method is giving the values that are in close agreement with the experimentally observed values.

It is obvious that the molecule 2-methoxy-*N*′-(2-methoxybenzoyl)benzohydrazide labelled as **11** whose chemical structure is given in Figure 27, does not show any type of self-dimerization or aggregation [134], even in 20 mM solution. The ^{1}H-DOSY [137,138] NMR experiment has therefore been carried out for a mixture of 1:1 molar ratio (20 mM final solution) of molecules **11** and **26** in the solvent $CDCl_3$ and the corresponding spectrum is reported in Figure 27.

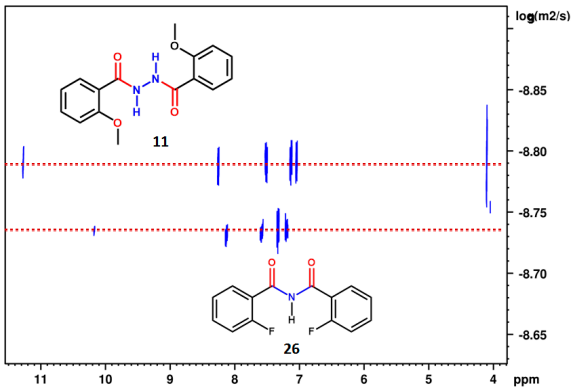

Figure 27. 500 MHz ^{1}H-DOSY NMR spectrum of 20 mM solution of the mixture of molecules **11** and **26** at a 1:1 molar ratio in $CDCl_3$.

The different diffusion coefficients detected for these two molecules discarded the possibility of self or cross dimerization. The triplet pattern was detected for the NH peak of the molecule **26** with the separation of 13.03 Hz between adjacent peaks. This triplet collapses into a singlet in ^{1}H{^{19}F} experiment confirming the presence of coupling between ^{1}H and ^{19}F. This has been further ascertained by acquiring the spectrum in a high polarity solvent DMSO-d_6 which resulted in the collapsing of triplet to a singlet confirming that this coupling is mediated through HB.

The visualization of coupling became more prominent in the 2D ^{1}H-^{15}N HSQC NMR experiment and the corresponding spectrum for molecule **26** is reported in Figure 28. The ^{1}H-^{15}N HSQC spectrum of the same molecule in the solvent DMSO-d_6 is reported in Figure 28c. In the solvent DMSO, except for $^{1}J_{NH}$, all the other couplings disappeared, giving strong and unambiguous evidence that the measured couplings $^{1h}J_{FH}$ and $^{2h}J_{FN}$ in the solvent $CDCl_3$ are mediated through HB. The ^{1}H-^{15}N HSQC spectra of all the other fluorine containing investigated molecules also exhibited through space couplings of different magnitudes.

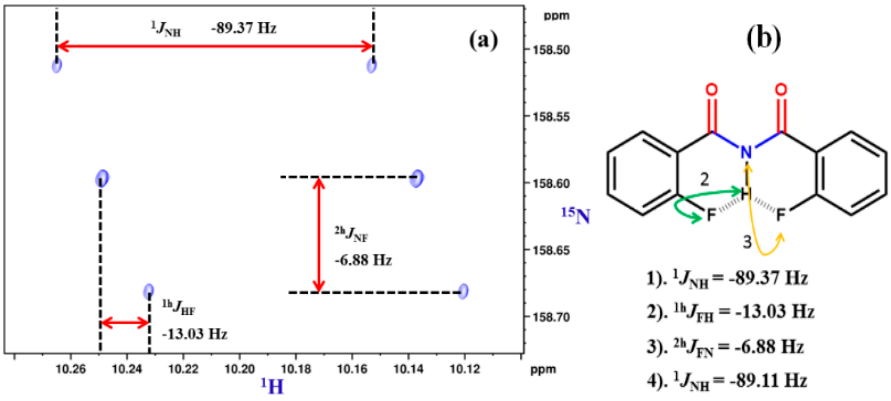

Figure 28. *Cont.*

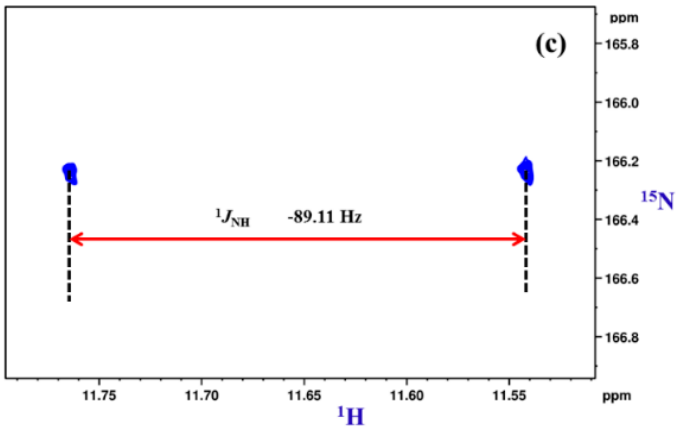

Figure 28. 800 MHz spectrum of molecule **26** in $CDCl_3$ (**a**) ^{1}H-^{15}N-HSQC (NH-coupled) spectrum; (**b**) the chemical structure of molecule **1** and measured couplings with their signs; (**c**) 400 MHz ^{1}H-^{15}N-HSQC spectrum (NH-coupled) in DMSO-d_6.

The $^1J_{NH}$ values of the molecules **26**, **27** and **29**–**32** are substantially smaller than the molecule **28**, providing strong and unambiguous evidence that the nature of HBs in the derivatives of imides is predominantly of the covalent type [143,144] The strong correlations in the 2D ^{1}H-^{19}F HOESY [163–165] experiments for the molecules **26** and **29**–**32** established the close proximity between NH and F atoms in these molecules. The 2D ^{1}H-^{19}F HOESY spectrum of the molecule **26** is reported in the Figure 29.

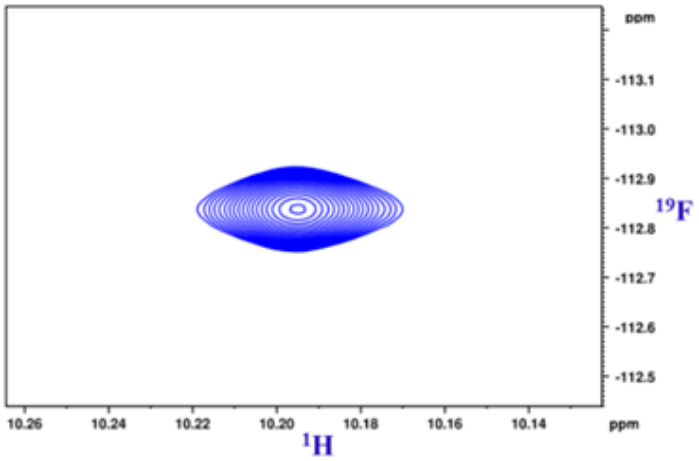

Figure 29. 376.5 MHz 2D ^{1}H-^{19}F HOESY spectrum of the molecule **26** in $CDCl_3$.

5.2. Theoretical Calculations

The DFT [135,136] optimized structure calculations have been carried out to ascertain the NMR observations. The DFT calculations have been performed with B3LYP/6-311+g (d,p) level of theory with the chloroform as the solvation medium. The energy minimized structures were confirmed by harmonic vibrational frequency. The wave function files for QTAIM, and NCI studies and simulated ^{1}H-NMR spectra using CSGT [145] were generated from optimized coordinates.

5.2.1. Conformational Study

For all the investigated imides maximum of 3–4 major conformations are possible due to ring flip as shown in the Figure 30.

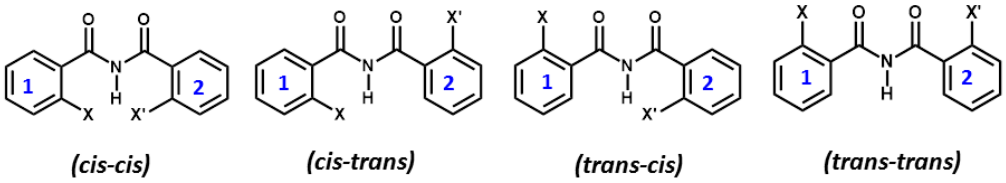

Figure 30. The possible conformers of the investigated imide molecules, arising due to the ring flip.

Out of the four possible conformers the cis-cis and trans-trans conformers were optimized and the difference {(*cis-cis*) – (*trans-trans*)} of minimum energy has been taken. The energy difference $\Delta E_{cis\text{-}trans}$ varied from approximately −2 to −11 Kcal/mol among all the investigated imide molecules and it is also found that the energy of *cis-cis* conformers is always lower than the *trans-trans* that are due to the presence of HB.

Relaxed Potential Energy Scan

The findings of *cis-cis* and *trans-trans* energies of the conformers has been further supported by relax potential energy scans. Relaxed potential energy surface for the internal rotation of the phenyl ring through single bond has been performed. The rotation of 360° (−180–0–+180) through single bond was scanned in 20 steps with 18° of rotational segments. The scanned graph of energy (kcal/mol) versus dihedral angle (θ°) is reported in Figure 31. From the graph, it is clear that the energy of the *cis* conformer is lower than the other, and the maximum is for the *trans* conformation.

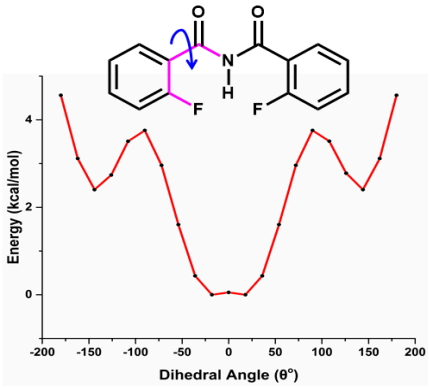

Figure 31. Relaxed potential energy surface for the internal rotation of the phenyl ring through single bond. The dihedral angle and rotation direction are highlighted in the structure of molecule **26**.

5.2.2. Non Covalent Interaction (NCI) Calculations

The grid points based on NCI [90] calculations have been plotted for a defined real space function, $sign(\lambda 2_{(r)})\rho_{(r)}$, as function 1 and reduced density gradient (RDG) as function 2 and color filed isosurfaces are plotted for the investigated molecules. The NCI studies provided the visual information about weak interactions and repulsions in the molecules [158].

5.2.3. Atoms in Molecules (AIM) Calculations

The magnitudes of $\rho_{(r)}$, signs of $\nabla^2\rho_{(r)}$ and potential energy density ($V_{(r)}$) at corresponding (3, −1) BCP (bond critical points) (r_{cp}) for HBs of interest have been calculated using QTAIM calculations [91–95]. The value of ($V_{(r)}$) used in the $E_{HB} = V(r_{bcp})/2$ [96] for the calculation of energy of HB (E_{HB}) of X···HX type. The calculated E_{HB} of different HBs in all the investigated molecules varied from −2 to −8.56 Kcal/mol [158]. The bond paths for (3, −1) BCPs were generated for the investigated molecules for visualization and the molecular model for the molecule **26** containing BCPs and bond path is reported in Figure 32.

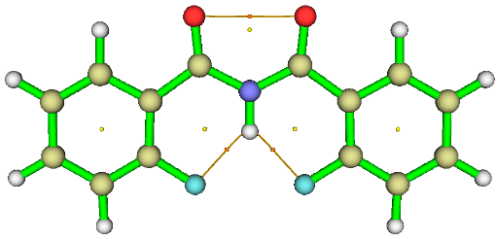

Figure 32. The visualization of BCPs and bond paths of HB for the molecule **26** plotted using the Multiwfn software. Dots represent the CPs and thin bar represents the HB interactions.

6. Studies on Diphenyloxamides

The existence of three centered C=O···H(N)···X-C HB involving organic fluorine, and other halogens in the derivatives of diphenyloxamide has been explored by NMR spectroscopy and quantum theoretical studies. The diphenyloxamide derivatives are the basic units of foldamers, where the formation of three centered HB contributes to the stable and rigid structure. The possible mode of three-centered HB formation C=O···H(N)···X-C (where X = CF_3, F, Cl, Br and I) in the investigated molecules, along with their chemical structures are given in Figure 33.

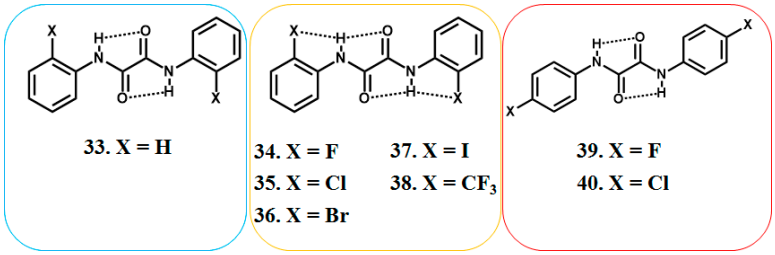

Figure 33. Chemical structures of *N*,*N*-diphenyloxamide (**33**) and its derivatives **34**–**40**. The dotted line3 indicate the HBs.

6.1. Experimental Observation by NMR Spectroscopy

Initial studies were focused on the concentration dependence of NH chemical shift (δ_{NH}) for all the molecules and it was observed that δ_{NH} remained unaltered for all the molecules, discarding the presence of any type of intermolecular interactions [166]. Compared to the unsubstituted molecule **33** the chemical shifts of NH protons are observed to be more deshielded for the different substituted molecules, **34**–**38**, indicating the participation of NH proton in weak molecular interactions [166]. The deshielding of NH chemical shift on lowering the temperature due to the strengthening in the HB is evident from Figure 34A.

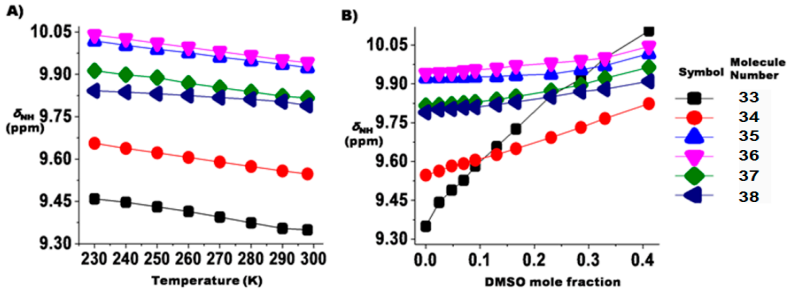

Figure 34. The variation of the chemical shift of NH proton (**A**) with temperature; (**B**) with the incremental addition of DMSO-d_6 to the solution containing 200 µL of $CDCl_3$. The 10 mM concentration at 298 K for the molecules, **33**–**38** has been initially taken for both the studies.

The high polarity solvent DMSO-d_6 induced perturbation of δ_{NH} is reported in Figure 34B. The larger value of $\Delta\delta_{NH}/\Delta V_{DMSO}$ in molecule **33** compared to the molecules, **34**–**38**, is giving an indication that the probable three centered H-bond is relatively stronger than the two centered one.

The 2D ^{15}N-^{1}H HSQC experiments for all the investigated molecules have been carried out, where ^{15}N is in natural abundance. The ^{15}N-^{1}H HSQC spectrum of molecule **38** in $CDCl_3$ yielded a quartet for the NH proton (reported in Figure 35B) implying that the rotation of CF_3 group is very fast unlike in the earlier reported studies [79]. The ^{15}N-^{1}H HSQC spectrum of molecule **34** in the solvent $CDCl_3$, reported in Figure 35A, yielded a doublet for the NH proton.

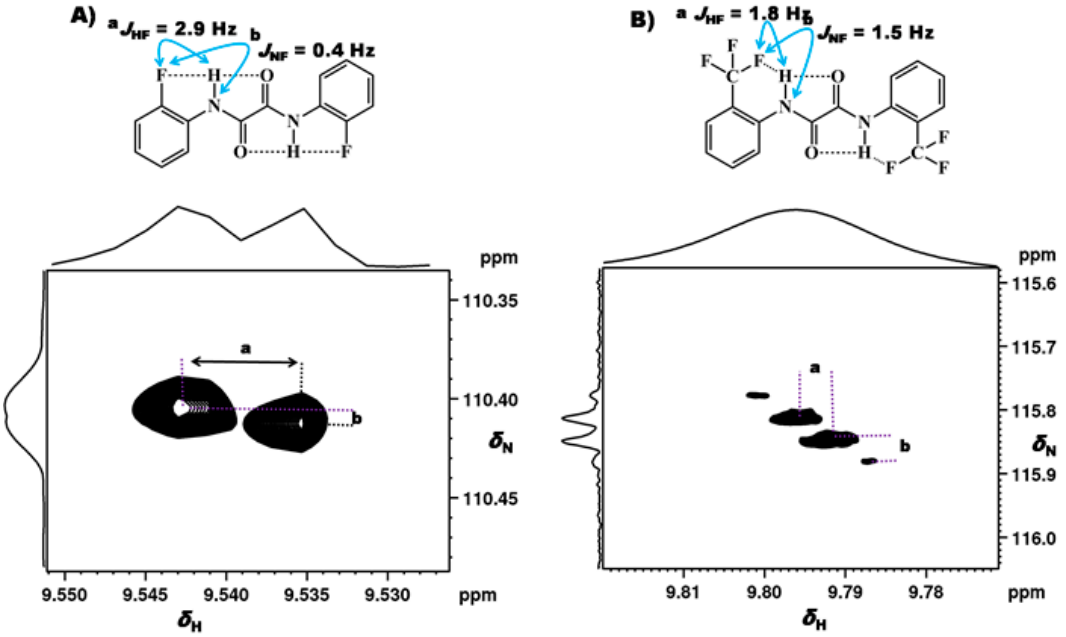

Figure 35. (**A**,**B**) ^{15}N-^{1}H-HSQC spectra of the molecules **34** and **38** respectively, in $CDCl_3$. The molecular structures and the measured couplings have also been reported.

The quartet in ^{15}N-^{1}H HSQC spectrum of molecule **38** which was observed in the solvent $CDCl_3$ collapsed to the singlet in the solvent DMSO-d_6 reported in Figure 36B. This unambiguously established the existence of HB in the molecule **38**.

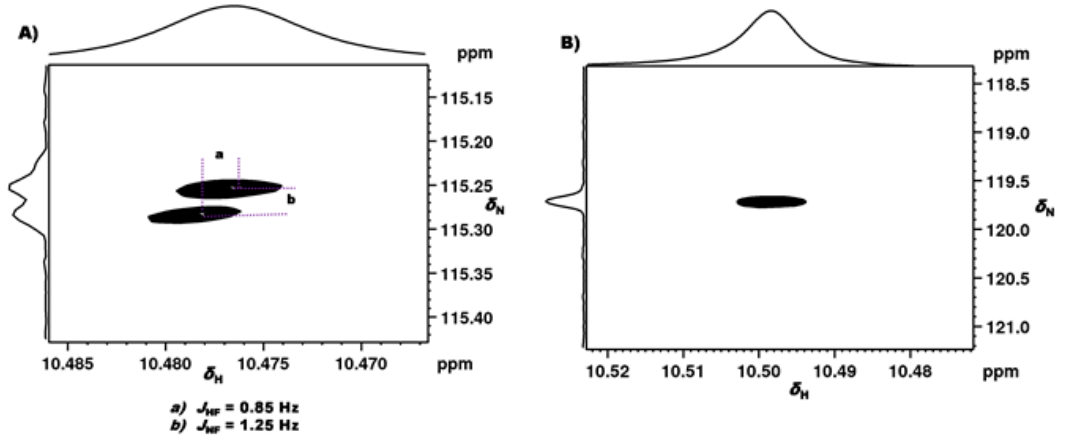

Figure 36. (**A**,**B**) ^{15}N-^{1}H HSQC spectra of the molecules **34** and **38** respectively, in DMSO-d_6.

The molecule **34** in solvent DMSO-d_6 yielded a doublet as reported in Figure 36A, with the J_{HF} = 0.85 Hz and J_{NF} = 1.25 Hz, whereas in $CDCl_3$ these values were J_{HF} = 2.9 Hz and J_{NF} = 0.4 Hz,

respectively. But it is observed that the relative slopes of the displacement vectors of the cross sections in the solvents (DMSO-d_6 or $CDCl_3$) are opposite (Figures 35A and 36A). As the HB gets ruptured in the high polar solvents, the couplings observed in the DMSO-d_6 are considered as through bond couplings and the observed coupling in the solvent $CDCl_3$ is considered as through space coupling. Hence the contribution from the HB alone turns out to be −3.75 Hz.

As far as signs of J_{NF} is concerned, it has to be negative. These observations gave a strong evidence for the presence of HB in the molecule **34**. The close proximity between fluorine atom and NH protons has also been confirmed by the detection of cross peak in the 2D ^{1}H-^{19}F HOESY spectra of molecules **34** and **38**. This is additional support for the presence of intramolecular HB between F and NH proton [166]. An increase in the $^1J_{NH}$ relative to molecule **33**, is observed in molecules **34**–**36** and **38**, indicating that the HB in these molecules is predominantly an electrostatic in nature [143,144]. On the other hand, $^1J_{NH}$ decreases in molecule **37**, hence the nature of HB is predominantly covalent in this molecule [40].

6.2. Theoretical Studies

The observed experimental results have been also corroborated by DFT based theoretical calculations, such as, QTAIM [91–95], Natural Bond Orbital (NBO) [159] and NCI [90].

6.2.1. QTAIM Calculations

The magnitude of electron density (ρ) and sign of Laplacian of electron density ($\nabla^2\rho$) are examined for the determination of HB. For such a purpose BCPs and bond paths for intramolecular HBs are detected for the investigated molecules and are reported in Figure 37.

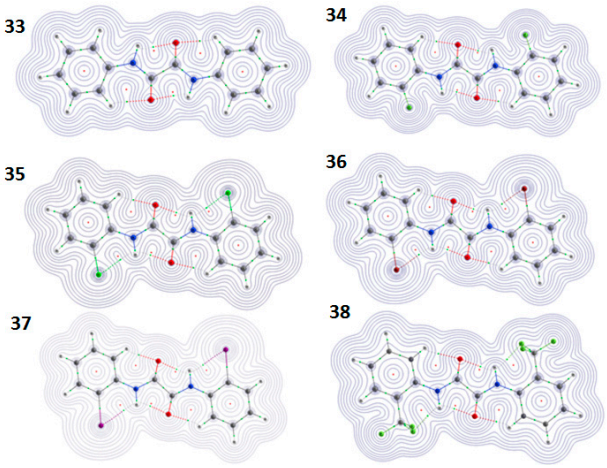

Figure 37. Molecular graphs, contour plots and AIM calculated bond paths for the molecules **33**–**38**. Dotted lines indicate the intramolecular HBs. Green and red dots are bond critical points (BCP) and ring critical points (RCP), respectively. Electron density is plotted as contours in the blue curves in the plane of molecules.

The observed electron density values fall in the expected range (0.0102–0.0642 a.u.) for HBs [167]. The positive sign of Laplacian of electron density ($\nabla^2\rho$) at the (3, −1) BCPs indicates the type of interactions that belong to the HBs. On the basis of electron density, the proton acceptance trend for organic halogens in the intramolecular five membered N-H···X follows the pattern Br > Cl > I, as detected from the chemical shift difference between the molecules **34**–**37** [166] compared to that of molecule **33**. This trend is further supported by the ρ(NH···X) values [166]. The obtained electron density values are about 0.015, 0.020 and 0.017 for NH···X, NH···O and CH···O, respectively. By using these values in the bonding energy (BE) equation; {BE (kj/mol) = 777 × ρ (in a.u.) − 0.4}, the BEs are estimated to be around 11, 15 and 13 kJ for NH···X, NH···O and CH···O HB interactions, respectively.

6.2.2. NBO Analysis

For HB formation, electron transfer from the electron rich region of HB acceptor to the anti-bonding orbital (σ*) of the HB donor takes place. This has been studied by the Natural Bond Orbital (NBO) analysis and found that the values of lp(O) → σ*(N-H) were always greater than the lp(O) → σ*(C-H) values. Hence the N-H···O bonds are concluded to be stronger than the C-H···O bonds.

6.2.3. NCI Analysis

QTAIM calculations and NBO analysis did not show the intramolecular BCP for N-H···F interaction in molecule **2** which contradicts the NMR observations. Another powerful method, NCI index has been used to visualize the weak interaction which showed the presence of HB in molecule **34**, which is in agreement with NMR observations. In Figure 38 (left side), the calculated grid points are plotted for the two functions: sign(λ_2)*ρ as function 1 and reduced density gradient (RDG) as function 2 by Multiwfn program. Color filled isosurface graphs are plotted using these grid points and are reported in the right side of the Figure 38.

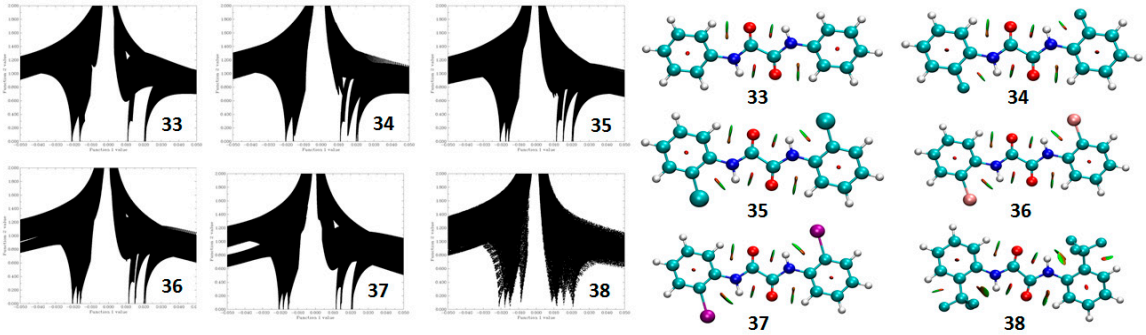

Figure 38. The plot of function 1 (sign(λ_2)*ρ values) on X-axis vs function 2, the reduced density gradient (RDG) on *Y*-axis. (left hand side), colored isosurface plots in which Green colour denotes weak HB and red color stands for steric effect. Labels 33–38 represent molecules **33**–**38**, respectively.

For the molecules **35**, **36**, and **37**, there are three spikes on the left-hand side which denote three HBs namely N-H···X, N-H···O and C-H···O (where X = Cl, Br, and I), these three bonds can be also seen in the colored isosurface plots reported on the right side of the Figure 38. For X = F, all three bonds exist and the spikes corresponds to two HBs are overlapped, these three HBs also are clearly seen in the isosurfaces plot 2. For X = CF_3, the four spikes have been seen that are also visible in isosurfaces plot 6.

6.2.4. Relaxed Potential Energy Scan

It may be pointed out that in the ^{15}N-^{1}H-HSQC NMR spectrum of molecule **38** the NH group appeared as a quartet due to fast rotation of CF_3 group at the ambient temperature. Relaxed potential energy scan for the H9–C5–C16–F2 dihedral angle was performed to derive the information about the energy barrier of internal rotation of CF_3 group. This is reported in the Figure 39.

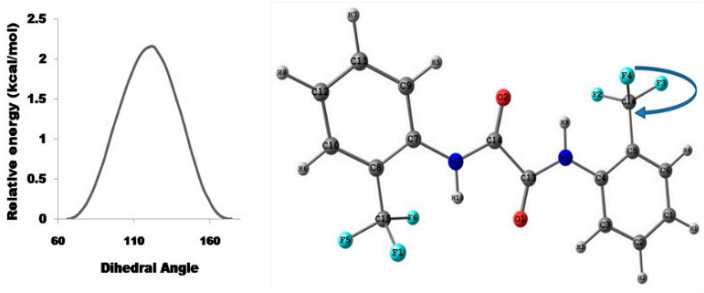

Figure 39. Relaxed potential energy surface for the internal rotation of CF_3 group at B3LYP/6-311G** level of calculation. The dihedral angle H9–C5–C16–F2 has been selected for the scan.

The barrier for this internal rotation was calculated as 2.15 kcal/mol using B3LYP/6-311G** level of theory and the energy barriers that can be observed in NMR is in between the 7–24 kcal/mol. This was the reason for observation of quartet for NH group.

7. Utility of H/D Exchange for Study of HB

The presence of HBs affects the release rate of labile hydrogen(s) which is/are participating in the reaction. There are number of chemical reactions in which the transfer of one or more protons (viz., hydride ions or hydrogen atoms) takes place in the rate determining step [40,42–45] The reaction kinetics depend on several factors, which also include the strength of intramolecular HB and the electronic effects caused by the substituents. The NMR spectroscopy is found to be a powerful technique which is widely employed for understanding the protein conformation, and dynamics [46–52] in aqueous media can be utilized to monitored by hydrogen/deuterium (H/D) exchange.

7.1. Factors Affecting the H/D Exchange

The rate of H/D exchange in a particular molecule can be affected by the inter- and the intra- molecular HBs. There will be a rapid exchange of the proton attached to nitrogen with the labile protons of the solvent. The mechanism of H/D exchange has been reported earlier in the derivatives of amides [53]. In the non-deuterated solvents, the proton exchange does not reflect in the NMR spectrum. On the other hand, in the presence of a labile deuterium-containing solvent the exchange takes place with the deuterium of the solvent molecules. This will have significant effect on the time dependent variation in the NMR signals intensities and permits the determination of H/D exchange rate. If the deuterated solvent is used in excess compared to the substrate, then the rate of exchange follows the pseudo first order kinetics. It is well known that the rate of H/D exchange is not only dependent on the strength of the intramolecular hydrogen bond, but also dependent on the electronic effect of the substituents.

The amides and amines are the basic building blocks for the synthesis of heterocyclic and linear nitrogen containing compounds. Consequent to significant difference in electronegativity (EN) and size among halogens, the strength of hydrogen bonds, steric hindrance and electronic effects [168] by these groups would also be substantially different. Hence the electronic effect, size effect and the effect of organic fluorine involved intramolecular HB on H/D exchange using ^{1}H-NMR spectroscopic techniques has also been explored in the different halo substituted anilines and benzamides [169]. The chemical structures of all the investigated molecules are reported in Figure 40.

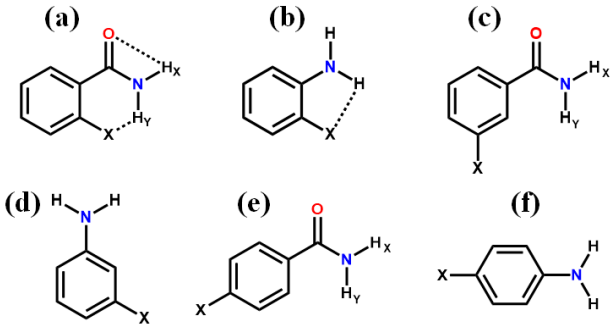

Figure 40. The general chemical structures of investigated halo substituted benzamides and anilines. For (**a**) and (**b**) X = F, Cl, Br, I and H and for (**c**), (**d**), (**e**), and (**f**) X = F, Cl and H.

For all investigated molecules the 5 mM stock solution was prepared on the volume scale of 5 mL in the fresh $CDCl_3$ solvent and the ^{1}H-NMR spectra have been obtained using 450 µL of this stock solution. To this solution 50 µL of CD_3OD was added with the marking time as zero, resulting in the final substrate concentration of less than 5 mM. This was well below the concentrations where the possibility of any aggregation and intermolecular interaction is observable. The added methanol created a 10% methanol:chloroform solution, with the final methanol concentration of 2.47 M, which ensured pseudo-first-order kinetics. The NMR spectra were acquired at every two minutes' interval until the amino proton signal intensity submerged within the baseline noise. A distinct non-exchangeable aromatic proton peak was used as an internal integration reference. Rate constants and corresponding half-lives were determined from the slope of a nonlinear least squares fit to the graph of $A(t) = A(o)\ exp^{(-kt)}$, rather than estimating the values at the extended time. The absolute intensity of Y intercept was taken 1 at zero time, and this value was used to normalize with respect to the remaining hydrogen. The X-intercept was the time. To ensure reproducibility the experiments have been repeated on a different sample at different time.

7.2. Exchange Mechanism

On addition of CD_3OD the labile protons undergo exchange with the hydroxy deuterium of the solvent molecule. This time dependent phenomenon followed the first order reaction kinetics and the intensity of the labile protons was systematically reduced. The mechanism of exchange is pictorially illustrated in Figure 41.

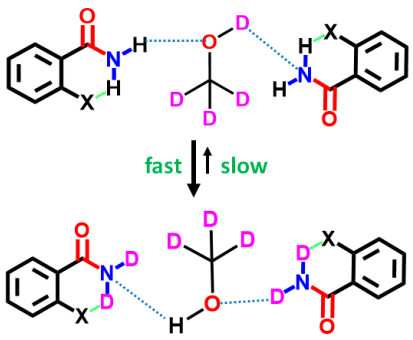

Figure 41. The mechanism of H/D exchange of labile protons with the hydroxy cdeuterium of the solvent molecule. The rate of deuteration is fast due to the high concentration of CD_3OD compared to substrate.

To get qualitative information about the strength of intramolecular HBs, and electronic effect the different halo substituted benzamide molecules were also investigated. The intensity of the peak

at zero time is taken as 100%. The other spectra were acquired after adding 50 μL of CD_3OD to 450 μL solution. The plot of integral areas of NH_2 peaks as a function of time, for unsubstituted and *ortho*-halosubstituted benzamides (2-fluoro, 2-chloro, 2-bromo, 2-iodo) are compared in Figure 42. Similar results for *meta*- and *para*-substituted derivatives have also been obtained [169].

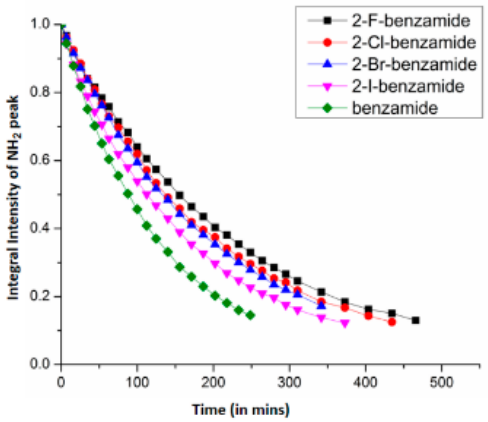

Figure 42. The plot of integral intensities of the NH_2 peaks v/s time (in mins) for unsubstituted and ortho-halosubstituted benzamides. The molecules are identified by the symbols given in inset.

The nature of the substituents dictated the H/D rate constants and they were different for different substituents. It has been observed that when all the physical parameters were kept unchanged for any of the investigated molecules, the results could be reproduced with high degree of accuracy within the experimental error [169]. There is a perfect match of graphical plots obtained from integral intensity of the labile protons peaks as a function of time, carried out for different samples at different times for 2-fluorobenzamide. This is clearly evident from Figure 43.

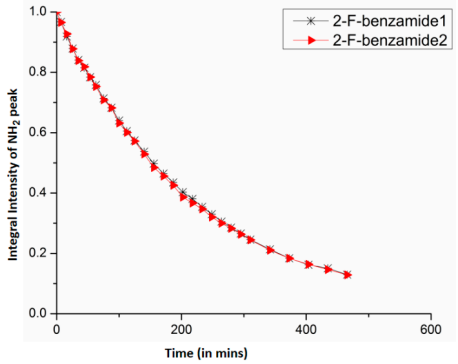

Figure 43. The integral intensity of NH_2 peaks v/s time (in minutes) for 2-fluorobenzamide plotted from two experiments carried out at different times intervals are represented by two different symbols, shown in the inset.

8. Multiple Quantum (MQ) NMR for the Detection of Intramolecular HBs

In deriving the evidence for C-F···H-N HB it is very important to know the precise magnitudes and also the relative signs of $^{1h}J_{FH}$, $^{3h}J_{FH}$, $^{2h}J_{FN}$ and $^{1}J_{NH}$ [65,69,170]. When three or more NMR active spins are coupled among themselves the magnitudes and signs of the couplings between the passive spins cannot be determined from the one-dimensional spectrum of any one of the coupled nuclei. Consequently, to obtain $^{2h}J_{FN}$ in organofluorine molecules several experimental strategies have been reported where ^{15}N is either isotopically labelled [111,170,171] or unlabelled [69].

8.1. The Pulse Sequence

The utilization of two dimensional ^{15}N-^{1}H correlation (HSQC) type experiments [172,173] gives information on the magnitudes of $^{1h}J_{FH}$, $^{3h}J_{FH}$, $^{2h}J_{FN}$ and $^{1}J_{NH}$ but fails to provide the signs of the passive couplings. Hence the multiple quantum NMR experimental methodology has been employed [174,175]. The application of two dimensional heteronuclear ^{15}N-^{1}H double quantum-single quantum (DQ-SQ) and zero quantum-single quantum (ZQ-SQ) correlation experiment, where ^{15}N is present in its natural abundance has been exploited for the determination of relative signs and magnitudes of the couplings among ^{1}H, ^{19}F and ^{15}N, involved in hydrogen bonding [169]. The pulse sequence utilized for DQ-SQ and ZQ-SQ experiments is well known and is reported in the Figure 44.

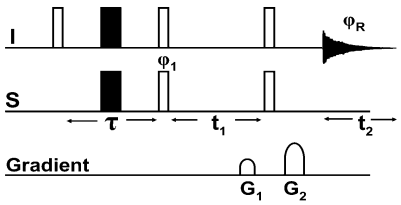

Figure 44. The pulse Sequence for DQ-SQ and ZQ-SQ experiments. For DQ and ZQ excitation, I and S spins are ^{1}H and ^{15}N of NH group. And the pulses were selective on these two spins. The phases of the pulses ϕ_1 and ϕ_R are x, −x, −x, x. The phase of all the remaining pulses are x. The gradients ratio G_1:G_2 employed are 50:55 for DQ-SQ and 50:45 for ZQ-SQ experiments. The τ delay for all the DQ-SQ and ZQ-SQ experiments and also ^{15}N-^{1}H HSQC experiments was optimized for $1/2J_{NH}$ (J_{NH} is taken to be 90 Hz).

The MQ experiments have been carried out on different fluorine substituted derivatives of benzamide in solution state in a low polarity solvent $CDCl_3$. The magnitudes and signs of through space and long range coupling interactions among fluorine, hydrogen and nitrogen nuclei in its natural abundance have been used to extract direct evidence for the existence of non-linear and/or three centered intra-molecular C-F···H-N type HB. The chemical structures and 1D ^{1}H-NMR spectra obtained for the investigated molecules are given in the Figure 45.

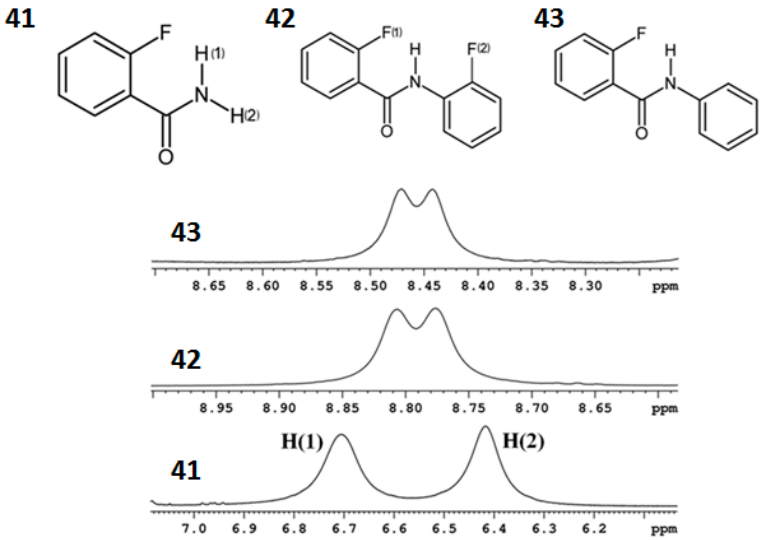

Figure 45. Chemical structures and expanded NH regions of the 1D ^{1}H-NMR spectra in $CDCl_3$ of 2-fluorobenzamide (**41**) 2-fluoro-*N*-(2-fluorophenyl)benzamide (**42**) and 2-fluoro-*N*-phenyl-benzamide (**43**).

Subsequently the theoretically derived results [63] have been employed in conjunction with NMR findings to draw the direct and unambiguous conclusions on the intra-molecular C-F···H-N type HB.

8.2. C-F···N-H Hydrogen Bond in 2-Fluorobenzamide

The two broad singlets with a separation of nearly 145 Hz observed in ^{1}H-NMR spectrum of molecule **41**, are attributed to two non-equivalent protons ($\delta_{NH(1)} > \delta_{NH(2)}$) [111]. The excessive broadening of the ^{1}H spectrum due to quadrupolar ^{14}N relaxation prevented the determination of through space and through bond couplings, if any. For visualization of such couplings if present, the heteronuclear ^{15}N-^{1}H DQ-SQ correlation experiments have been carried out using the pulse sequence given in Figure 36 [176,177]. The ^{15}N-^{1}H DQ-SQ correlated spectrum is reported in Figure 37, where DQ coherence evolve at the algebraic sum of the couplings between active (^{1}H, ^{15}N) and passive (^{19}F) spins. Nearly equal $^{1}J_{NH}$ of each amide proton permitted the simultaneous excitation and detection of two different ^{15}N-^{1}H DQ spectra and are identified by the groups marked N-H(1) and N-H(2) in Figure 46.

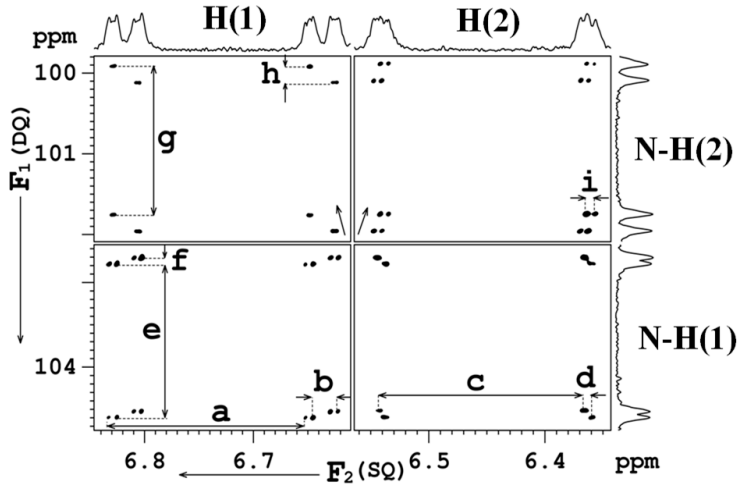

Figure 46. 500 MHz ^{15}N-^{1}H DQ-SQ spectrum of molecule **41** in the solvent $CDCl_3$.

For N-H(1) DQ excitation, H(1) and ^{15}N are the active spins and H(2) and ^{19}F are passive spins, while for N-H(2) DQ, H(2) and ^{15}N are the active spins and H(1) and ^{19}F are passive spins. The SQ dimension yields the normal spectrum of four coupled spins, viz., ^{15}N, ^{19}F and two NH protons. The nuclei involved in the DQ coherence flip simultaneously and can be treated as a single spin, also called as super spin [178]. The ^{19}F and ^{1}H being passive spins, the four possible spin states yield four transitions. The ^{15}N-^{1}H(1) DQ coherence gives the parameters $^{1h}J_{FH(1)}$, $^{2h}J_{FN}$, $^{2}J_{H(1)H(2)}$ and $^{1}J_{NH(2)}$ while ^{15}N-^{1}H(2) DQ coherence yields $^{3h}J_{FH(2)}$, $^{2h}J_{FN}$, $^{2}J_{H(1)H(2)}$ and $^{1}J_{NH(1)}$. The marked separations in the SQ dimensions of Figure 37 yield couplings (in Hz); a = $^{1}J_{NH(1)}$ (90.5), c = $^{1}J_{NH(2)}$ (89.2) and i = $^{2}J_{H(1)H(2)}$ (3.05 Hz). The separations in DQ dimension provide magnitudes of the couplings (in Hz), g = $^{1}J_{NH(1)}$ + $^{2}J_{H(1)H(2)}$ (93.5), e = $^{1}J_{NH(2)}$ + $^{2}J_{H(1)H(2)}$ (92.2), f = $^{1h}J_{FH(1)}$ + $^{2h}J_{FN}$ (3.8) and h = $^{3h}J_{FH(2)}$ + $^{2h}J_{FN}$ (10.4). The displacement of F_2 cross sections yield respectively (in Hz), b = $^{1h}J_{FH(1)}$ (11.2) and d = $^{3h}J_{FH(2)}$ (3.0). Opposite directions of F_1 displacement vectors at $\delta_{H(1)}$ and $\delta_{H(2)}$, denoted by tilted arrows, confirm opposite signs of $^{1h}J_{FH(1)}$ and $^{3h}J_{FH(2)}$ [177,179]. The signs of $^{1}J_{NH(1)}$ and $^{1}J_{NH(2)}$ are negative because of the convention that one bond scalar coupling between two nuclei of opposite signs of magnetic moments is negative. The algebraic combination of parameters obtained from the DQ spectrum established that the relative signs of $^{1h}J_{FH(1)}$ and $^{3h}J_{FH(2)}$ are opposite, that of $^{1h}J_{FH(1)}$, $^{2h}J_{FN}$ and $^{1}J_{NH}$ are same (negative), $^{2}J_{H(1)H(2)}$ is positive. Thus, the magnitudes and relative signs of the couplings among all the three nuclei could be obtained from a single 2D NMR experiment. This information can be utilized for ascertaining the existence of C-F···H-N hydrogen bonding, if any,

utilizing the theoretical results [63]. Nevertheless, for unequivocally ascertaining the relative signs of $^{1h}J_{FH(1)}$, $^{3h}J_{FH(2)}$ and $^{2h}J_{FN}$, the ^{15}N-^{1}H zero quantum ^{15}N-^{1}H ZQ-SQ correlation experiment has also been carried out using the identical pulse sequence with appropriate gradient ratio and phases of the pulses. The ZQ coherence evolves at the algebraic difference of the couplings between active (^{1}H, ^{15}N) and passive (^{19}F) spins. Consequent to the opposite signs of magnetic moments of excited spins the coherence evolved as algebraic sums [180]. This resulted in the enhanced separation along the ZQ dimension of ZQ-SQ spectrum given in Figure 47.

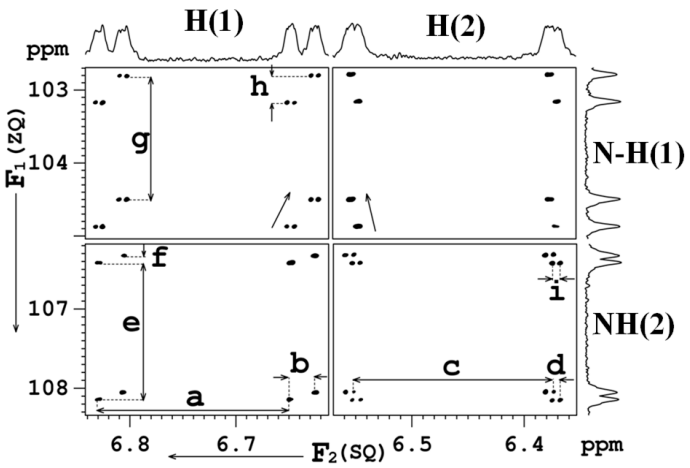

Figure 47. 500 MHz ^{15}N-^{1}H ZQ-SQ spectrum of **41** in $CDCl_3$.

It is evident that signs of $^{1h}J_{FH(1)}$ and $^{2h}J_{FN}$ are opposite to $^{3h}J_{FH(2)}$. The similar studies have also been carried out for other molecules and the obtained results established the presence of fluorine involved intramolecular HB.

9. Conclusions

The combined NMR experimental observations and various DFT based theoretical calculations revealed the existence of intramolecular HBs in different organofluorine-substituted derivatives of different classes of molecules, viz. benzanilides, hydrazides, imides, benzamides, and diphenyloxamides. The existence of more than one conformer has also been established in several molecules by adopting diverse NMR experimental strategies. In many examples the solvent titration and ^{1}H DOSY techniques are employed to discount any possibility of self- or cross-dimerization. The variable temperature and solvent titration studies provided the valuable information about the existence of HB, and their relative strengths. The ^{1}H-^{19}F HOESY experiment is utilized to extract the information about the spatial proximity and possibility of intramolecular HB, as well as for the determination of different conformers. Through space coupling between two NMR active nuclei, where the spin polarization is transmitted through HB of diverse strengths has been detected in several fluorine containing molecules. The 2D ^{1}H-^{15}N HSQC experiment aided in the measurement of coupling strengths and their relative signs. The weak molecular interactions established by NMR studies have also been corroborated by theoretical DFT based structure calculations. The NCI analysis served as a very sensitive tool for the detection of non-covalent interactions. NCI analysis provides the visual evidence for the presence of bi and trifurcated HBs in some of the molecules. For the calculation of strengths of different HBs in the investigated molecules the QTAIM calculation is found to be very powerful tool. The Laplacian of electron density sign is used to discriminate the HBs from the covalent bonds. The relaxed potential energy scan has been performed for some of the molecules to determine the free rotation energy of CF_3 group and the energies of different possible conformers for a molecule. The quantum calculations and classical MD simulations have supported the various possible ways of intramolecular HB formation with fluorine atom. The use of H/D exchange rates obtained by

conventional ^{1}H-NMR spectroscopic studies confirms the presence or absence of intramolecular HBs, and permitted the calculation of their relative strengths. The effect of inherent electronic and steric effects is also successfully correlated with the relative rates of H/D exchange in the various halo substituted derivatives of anilines and benzamides. The utilization of heteronuclear ^{15}N-^{1}H DQ-SQ and ZQ-SQ correlation experiment, in isotopically unlabeled systems for the detection of organic fluorine involved intramolecular HB and unequivocal determination of relative signs and magnitudes of both hydrogen bond and covalent bond mediated through scalar couplings such as $^{1h}J_{FH}$, $^{2h}J_{FN}$ and $^{3h}J_{FH}$ has been convincingly demonstrated.

10. Computational Methods and the Employed Programs

For DFT calculations Gaussian G09 [181] suite of programs has been used. The B3LYP/6-311G** and aug-cc-pVTZ level of theories and basis sets were used to optimize the structures of the molecules. To ensure that all optimized structures are global minima, harmonic vibrational frequency calculation has been performed at the same level of theories and all the real frequencies indicated that optimized geometry is minimum at potential energy surface. The MD simulations were performed using NAMD simulation package [182]. The general AMBER force field (GAFF) along with torsion parameters and partial charges obtained from quantum calculations in vacuum. The long range electrostatic interactions were calculated with the Particle Mesh Ewald (PME) method [183]. Constant pressure-temperature (NPT) simulation is performed followed by constant volume-temperature (NVT) simulation. AIMAll [184] and multiwfn programs were used for QTAIM calculations. Multiwfn [185] program was used for NCI plots. Colour filled isosurface graphs have been plotted by VMD [186] program. Specific combination of methods for theoretical calculations was used for particular and individual series of molecules, the specific information is available with the native articles. Molden 4.7 has been used as a visualization software for Gaussian outputs [187].

Acknowledgments: NS gratefully acknowledges the generous financial support by the Science and Engineering Research Board (SERB), New Delhi (Grant Number: EMR/2015/002263).

Conflicts of Interest: The authors declare no conflict of interest.

References

1. Müller-Dethlefs, K.; Hobza, P. Noncovalent Interactions: A Challenge for Experiment and Theory. *Chem. Rev.* **2000**, *100*, 143–167. [CrossRef] [PubMed]
2. Kaplan, I.G. *Intermolecular Interactions: Physical Picture, Computational Methods and Model Potentials*; John Wiley & Sons, Ltd.: New York, NY, USA, 2006.
3. Huggins, M.L. Quantum Mechanics of the Interaction of Gravity with Electrons: Theory of a Spin-two Field Coupled to Energy. PhD. Thesis, University of California, Oakland, CA, USA, 1919.
4. Huggins, M.L. Atomic structure. *Science* **1922**, *55*, 459–460. [CrossRef]
5. Huggins, M.L. Electronic Structures of Atoms. *J. Phys. Chem.* **1921**, *26*, 601–625. [CrossRef]
6. Huggins, M.L. Atomic radii. *Phys. Rev.* **1922**, *19*, 346–353. [CrossRef]
7. Latimerand, W.M.; Rodebush, W.H. Polarity and ionization from the standpoint of the Lewis theory of valence. *J. Am. Chem. Soc.* **1920**, *42*, 1419–1433. [CrossRef]
8. Hu, W.H.; Huang, K.-W.; Chiou, C.W.; Kuo, S.W. Complementary Multiple Hydrogen Bonding Interactions Induce the Self-Assembly of Supramolecular Structures from Heteronucleobase-Functionalized Benzoxazine and Polyhedral Oligomeric Silsesquioxane Nanoparticles. *Macromolecules* **2012**, *45*, 9020–9028. [CrossRef]
9. Saccone, M.; Dichiarante, V.; Forni, A.; Goulet-Hanssens, A.; Cavallo, G.; Vapaavuori, J.; Terraneo, G.; Barrett, C.J.; Resnati, G.; Metrangolo, P.; Priimagi, A. Supramolecular hierarchy among halogen and hydrogen bond donors in light-induced surface patterning. *J. Mater. Chem. C* **2015**, *3*, 759–768. [CrossRef]
10. Teunissen, A.J.P.; Nieuwenhuizen, M.M.L.; Rodríguez-Llansola, F.; Palmans, A.R.A.; Meijer, E.W. Mechanically Induced Gelation of a Kinetically Trapped Supramolecular Polymer. *Macromolecules* **2014**, *47*, 8429–8436. [CrossRef]

11. Xiao, T.; Feng, X.; Ye, S.; Guan, Y.; Li, S.L.; Wang, Q.; Ji, Y.; Zhu, D.; Hu, X.; Lin, C.; Pan, Y.; Wang, L. Highly Controllable Ring−Chain Equilibrium in Quadruply Hydrogen Bonded Supramolecular Polymers. *Macromolecules* **2012**, *45*, 9585–9594. [CrossRef]
12. Ajayaghosh, A.; George, S.J.; Schenning, A.P.H.J. Hydrogen-Bonded Assemblies of Dyes and Extended π-Conjugated Systems. In *Topics in Current Chemistry*; Würthner, F., Ed.; Springer: Berlin/Heidelberg, Germany, 2005; Volume 258, pp. 83–118.
13. Archer, E.A.; Gong, H.; Krische, M.J. Hydrogen bonding in noncovalent synthesis: selectivity and the directed organization of molecular strands. *Tetrahedron* **2001**, *57*, 1139–1159. [CrossRef]
14. Brunsveld, L.; Folmer, B.J.B.; Meijer, E.W.; Sijbesma, R.P. Supramolecular Polymers. *Chem. Rev.* **2001**, *101*, 4071–4098. [CrossRef]
15. Conn, M.M.; Rebek, J. Self-Assembling Capsules. *Chem. Rev.* **1997**, *97*, 1647–1668. [CrossRef] [PubMed]
16. Huang, F.; Gibson, H.W. Polypseudorotaxanes and polyrotaxanes. *Prog. Polym. Sci.* **2005**, *30*, 982–1018. [CrossRef]
17. Lawrence, D.S.; Jiang, T.; Levett, M. Self-Assembling Supramolecular Complexes. *Chem. Rev.* **1995**, *95*, 2229–2260. [CrossRef]
18. Lukin, O.; Vögtle, F. Knotting and Threading of Molecules: Chemistry and Chirality of Molecular Knots and Their Assemblies. *Angew. Chem. Int. Ed.* **2005**, *44*, 1456–1477. [CrossRef] [PubMed]
19. Nowick, J.S. Chemical Models of Protein β-Sheets. *Acc. Chem. Res.* **1999**, *32*, 287–296. [CrossRef]
20. Prins, L.J.; Reinhoudt, D.N.; Timmerman, P. Noncovalent Synthesis Using Hydrogen Bonding. *Angew. Chem. Int. Ed.* **2001**, *40*, 2382–2426. [CrossRef]
21. Schmuck, C.; Wienand, W. Self-Complementary Quadruple Hydrogen-Bonding Motifs as a Functional Principle: From Dimeric Supramolecules to Supramolecular Polymers. *Angew. Chem. Int. Ed.* **2001**, *40*, 4363–4369. [CrossRef]
22. Shenhar, R.; Rotello, V.M. Polymers Nanoparticles: Scaffolds and Building Blocks. *Acc. Chem. Res.* **2003**, *36*, 549–561. [CrossRef] [PubMed]
23. Sijbesma, R.P.; Meijer, E.W. Quadruple hydrogen bonded systems. *Chem. Commun.* **2003**, 5–16. [CrossRef]
24. Zeng, F.; Zimmerman, S.C. Dendrimers in Supramolecular Chemistry: From Molecular Recognition to Self-Assembly. *Chem. Rev.* **1997**, *97*, 1681–1712. [CrossRef] [PubMed]
25. Liu, X.-H.; Wang, D.; Wan, L.J. Surface Tectonics of Nanoporous Networks of Melamine-Capped Molecular Building Blocks formed through Interface Schiff-Base Reactions. *Chem. Asian J.* **2013**, *8*, 2466–2470. [CrossRef] [PubMed]
26. Rotondi, K.S.; Gierasch, L.M. Natural Polypeptide Scaffolds: β-Sheets, β-Turns, and β-Hairpins. *Pept. Sci.* **2006**, *84*, 13–22. [CrossRef] [PubMed]
27. Seebach, D.; Hook, D.F.; Glättli, A. Helices and Other Secondary Structures of β- and γ-Peptides. *Pept. Sci.* **2006**, *84*, 23–37. [CrossRef] [PubMed]
28. Užarević, K.; Đilović, I.; Bregović, N.; Tomišić, V.; Matković-Čalogović, D.; Cindrić, M. Anion-Templated Supramolecular C3 Assembly for Efficient Inclusion of Charge-Dispersed Anions into Hydrogen-Bonded Networks. *Chem. Eur. J.* **2011**, *17*, 10889–10897. [CrossRef] [PubMed]
29. Venugopalan, P.; Kishore, R. Unusual Folding Propensity of an Unsubstituted β,γ-Hybrid Model Peptide: Importance of the C–H···O Intramolecular Hydrogen Bond. *Chem. Eur. J.* **2013**, *19*, 9908–9915. [CrossRef] [PubMed]
30. Cougnon, F.B.L.; Sanders, J.K.M. Evolution of Dynamic Combinatorial Chemistry. *Acc. Chem. Res.* **2011**, *45*, 2211–2221. [CrossRef] [PubMed]
31. Goodman, C.M.; Choi, S.; Shandler, S.; DeGrado, W.F. Hydrothermal contribution to the oceanic dissolved iron inventory. *Nat. Chem. Biol.* **2007**, *3*, 252–256. [CrossRef] [PubMed]
32. Nowick, J.S. What I have learned by using chemical model systems to study biomolecular structure and interactions. *Org. Biomol. Chem.* **2006**, *4*, 3869–3885. [CrossRef] [PubMed]
33. Altintas, O.; Lejeune, E.; Gerstel, P.; Barner-Kowollik, C. Bioinspired dual self-folding of single polymer chains via reversible hydrogen bonding. *Polym. Chem.* **2012**, *3*, 640–651. [CrossRef]
34. Moure, A.; Sanclimens, G.; Bujons, J.; Masip, I.; Alvarez-Larena, A.; Pérez-Payá, E.; Alfonso, I.; Messeguer, A. Chemical Modulation of Peptoids: Synthesis and Conformational Studies on Partially Constrained Derivatives. *Chem. Eur. J.* **2011**, *17*, 7927–7939. [CrossRef] [PubMed]

35. Mingozzi, M.; Dal Corso, A.; Marchini, M.; Guzzetti, I.; Civera, M.; Piarulli, U.; Arosio, D.; Belvisi, L.; Potenza, D.; Pignataro, L.; Gennari, C. Cyclic *iso*DGR Peptidomimetics as Low-Nanomolar $\alpha_v\beta_3$ Integrin Ligands. *Chem. Eur. J.* **2013**, *19*, 3563–3567. [CrossRef] [PubMed]
36. Rufo, C.M.; Moroz, Y.S.; Moroz, O.V.; Stöhr, J.; Smith, T.A.; Hu, X.; DeGrado, W.F.; Korendovych, I.V. Short peptides self-assemble to produce catalytic amyloids. *Nat. Chem.* **2014**, *6*, 303–309. [CrossRef] [PubMed]
37. Wennemers, H. Asymmetric catalysis with peptides. *Chem. Commun.* **2011**, *47*, 12036–12041. [CrossRef] [PubMed]
38. Vagner, J.; Qu, H.; Hruby, V.J. Peptidomimetics, a synthetic tool of drug discovery. *Curr. Opin. Chem. Biol.* **2008**, *12*, 292–296. [CrossRef] [PubMed]
39. Ripka, A.S.; Rich, D.H. Peptidomimetic design. *Curr. Opin. Chem. Biol.* **1998**, *2*, 441–452. [CrossRef]
40. Dingley, A.J.; Masse, J.E.; Peterson, R.D.; Barfield, M.; Feigon, J.; Grzesiek, S. Internucleotide Scalar Couplings Across Hydrogen Bonds in Watson-Crick and Hoogsteen Base Pairs of a DNA Triplex. *J. Am. Chem. Soc.* **1999**, *121*, 6019–6027. [CrossRef]
41. Fonseca-Guerra, C.; Bickelhaupt, F.M.; Snijders, J.G.; Baerends, E.J. Hydrogen Bonding in DNA Base Pairs: Reconciliation of Theory and Experiment. *J. Am. Chem. Soc.* **2000**, *122*, 4117–4128. [CrossRef]
42. Smith, J.D.; Cappa, C.D.; Wilson, K.R.; Cohen, R.C.; Geissler, P.L.; Saykally, R.J. Unified description of temperature-dependent hydrogen-bond rearrangements in liquid water. *Proc. Natl. Acad. Sci. USA* **2005**, *102*, 14171–14174. [CrossRef] [PubMed]
43. Liskamp, R.M.J.; Rijkers, D.T.S.; Kruijtzer, J.A.; Kemmink, W.J. Peptides and Proteins as a Continuing Exciting Source of Inspiration for Peptidomimetics. *Chembiochem* **2011**, *12*, 1626–1653. [CrossRef] [PubMed]
44. Panciera, M.; Amorín, M.; Castedo, L.; Granja, J.R. Design of Stable b-Sheet-Based Cyclic Peptide Assemblies Assisted by Metal Coordination: Selective Homo- and Heterodimer Formation. *Chem. Eur. J.* **2013**, *19*, 4826–4834. [CrossRef] [PubMed]
45. Tremey, E.; Bonnot, F.; Moreau, Y.; Berthomieu, C.; Desbois, A.; Favaudon, V.; Blondin, G.; Houée-Levin, C.; Nivière, V. Hydrogen bonding to the cysteine ligand of superoxide reductase: Acid–base control of the reaction intermediates. *J. Biol. Inorg. Chem.* **2013**, *18*, 815–830. [CrossRef] [PubMed]
46. Wang, D.; Chen, K.; Kulp, J.L.; Arora, P.S. Evaluation of Biologically Relevant Short r-Helices Stabilized by a Main-Chain Hydrogen-Bond Surrogate. *J. Am. Chem. Soc.* **2006**, *128*, 9248–9256. [CrossRef] [PubMed]
47. Ko, E.; Liu, J.; Perez, L.M.; Lu, G.; Schaefer, A.; Burgess, K. Universal Peptidomimetics. *J. Am. Chem. Soc.* **2010**, *133*, 462–477. [CrossRef] [PubMed]
48. Jo, H.; Meinhardt, N.; Wu, Y.; Kulkarni, S.; Hu, X.; Low, K.E.; Davies, P.L.; DeGrado, W.F.; Greenbaum, D.C. Development of α-Helical Calpain Probes by Mimicking a Natural Protein−Protein Interaction. *J. Am. Chem. Soc.* **2012**, *134*, 17704–17713. [CrossRef] [PubMed]
49. Gross, E.; Liu, J.H.; Alayoglu, S.; Marcus, M.A.; Fakra, S.C.; Toste, F.D.; Somorjai, G.A. Asymmetric Catalysis at the Mesoscale: Gold Nanoclusters Embedded in Chiral Self-Assembled Monolayer as Heterogeneous Catalyst for Asymmetric Reactions. *J. Am. Chem. Soc.* **2013**, *135*, 3881–3886. [CrossRef] [PubMed]
50. Hammond, M.C.; Bartlett, P.A. Synthesis of Amino Acid-Derived Cyclic Acyl Amidines for Use in β-Strand Peptidomimetics. *J. Org. Chem.* **2007**, *72*, 3104–3107. [CrossRef] [PubMed]
51. Emenike, B.U.; Liu, A.T.; Naveo, E.P.; Roberts, J.D. Substituent Effects on Energetics of Peptide-Carboxylate Hydrogen Bonds as Studied by ^{1}H NMR Spectroscopy: Implications for Enzyme Catalysis. *J. Org. Chem.* **2013**, *78*, 11765–11771. [CrossRef] [PubMed]
52. Linton, B.R.; Reutershan, M.H.; Aderman, C.M.; Richardson, E.A.; Brownell, K.R.; Ashley, C.W.; Evans, C.A.; Miller, S.J. Asymmetric Michael addition of α-nitro-ketones using catalytic peptides. *Tetrahedron Lett.* **2007**, *48*, 1993–1997. [CrossRef]
53. Ghorai, A.; Padmanaban, E.; Mukhopadhyay, C.; Achari, B.; Chattopadhyay, P. Design and synthesis of regioisomeric triazole based peptidomimetic macrocycles and their dipole moment controlled self-assembly. *Chem. Commun.* **2012**, *48*, 11975–11977. [CrossRef] [PubMed]
54. Gong, B. Crescent Oligoamides: From Acyclic "Macrocycles" to Folding Nanotubes. *Chem. Eur. J.* **2001**, *7*, 4336–4342. [CrossRef]
55. Huc, I. Aromatic Oligoamide Foldamers. *Eur. J. Org. Chem.* **2004**, *1*, 17–29. [CrossRef]
56. Li, Z.T.; Hou, J.L.; Li, C.; Yi, H.P. Shape-Persistent Aromatic Amide Oligomers: New Tools for Supramolecular Chemistry. *Chem. Asian J.* **2006**, *1*, 766–778. [CrossRef] [PubMed]

57. Lockman, J.W.; Paul, N.M.; Parquette, J.R. The role of dynamically correlated conformational equilibria in the folding of macromolecular structures. A model for the design of folded dendrimers. *Prog. Polym. Sci.* **2005**, *30*, 423–452. [CrossRef]
58. Sanford, A.R.; Yamato, K.; Yang, X.; Yuan, L.; Han, Y.; Gong, B. Well-defined secondary structures, Information-storing molecular duplexes and helical foldamers based on unnatural peptide backbones. *Eur. J. Biochem.* **2004**, *271*, 1416–1425. [CrossRef] [PubMed]
59. Chopra, D. Is Organic Fluorine Really "Not" Polarizable? *Cryst. Growth Des.* **2012**, *12*, 541–546. [CrossRef]
60. Dunitz, J.D. Organic Fluorine: Odd Man Out. *ChemBioChem* **2004**, *5*, 614–621. [CrossRef] [PubMed]
61. Dunitz, J.D.; Taylor, R. Organic Fluorine Hardly Ever Accepts Hydrogen Bonds. *Chem. Eur. J.* **1997**, *3*, 89–98. [CrossRef]
62. Howard, J.A.K.; Hoy, V.J.; O'Hagan, D.; Smith, G.T. How Good is Fluorine as a Hydrogen Bond Acceptor? *Tetrahedron* **1996**, *52*, 12613–12622. [CrossRef]
63. Alkorta, I.; Elguero, J.; Limbach, H.H.; Shenderovich, I.G.; Winkler, T. A DFT and AIM analysis of the spin–spin couplings across the hydrogen bond in the 2-fluorobenzamide and related compounds. *Magn. Reson. Chem.* **2009**, *47*, 585–592. [CrossRef] [PubMed]
64. Bartolome, C.; Espinet, P.; Martin-Alvarez, J.M. Is there any bona fide example of O–H···F–C bond in solution? The cases of $HOC(CF_3)_2$(4-X-2,6-$C_6H_2(CF_3)_2$) (X = Si(*i*-Pr)$_3$, CF_3). *Chem. Commun.* **2007**, 4384–4386. [CrossRef] [PubMed]
65. Kareev, I.E.; Quiñones, G.S.; Kuvychko, I.V.; Khavrel, P.A.; Ioffe, I.N.; Goldt, I.V.; Lebedkin, S.F.; Seppelt, K.; Strauss, S.H.; Boltalina, O.V. Variable-Temperature ^{19}F NMR and Theoretical Study of 1,9- and 1,7-$C_{60}F(CF_3)$ and C_S- and C_1-$C_{60}F_{17}(CF_3)$: Hindered CF_3 Rotation and Through-Space J_{FF} Coupling. *J. Am. Chem. Soc.* **2005**, *127*, 11497–11504. [CrossRef] [PubMed]
66. Prakash, G.K.S.; Wang, F.; Rahm, M.; Shen, J.; Ni, C.; Haiges, R.; Olah, G.A. On the Nature of C-H···F-C Interactions in Hindered CF-C(sp3) Bond Rotations. *Angew. Chem. Int. Ed.* **2011**, *50*, 11761–11764. [CrossRef] [PubMed]
67. Ledbetter, M.P.; Saielli, G.; Bagno, A.; Tran, N.; Romalis, M.V. Observation of scalar nuclear spin–spin coupling in van der Waals complexes. *Proc. Natl. Acad. Sci. USA* **2012**, *109*, 12393–12397. [CrossRef]
68. Saielli, G.; Bini, R.; Bagno, A. Computational ^{19}F-NMR. 2. Organic compounds. *RSC. Adv.* **2014**, *4*, 41605–41611. [CrossRef]
69. Rae, I.D.; Weigold, J.A.; Contreras, R.H.; Biekofsky, R.R. Analysis of Long-Range Through-Space Couplings via an Intramolecular Hydrogen Bond. *Magn. Reson. Chem.* **1993**, *31*, 836–840. [CrossRef]
70. Benedict, H.; Shenderovich, I.G.; Malkina, O.L.; Malkin, V.G.; Denisov, G.S.; Golubev, N.S.; Limbach, H.H. Nuclear Scalar Spin-Spin Couplings and Geometries of Hydrogen Bonds. *J. Am. Chem. Soc.* **2000**, *122*, 1979–1988. [CrossRef]
71. Golubev, N.S.; Shenderovich, I.G.; Smirnov, S.N.; Denisov, G.S.; Limbach, H.-H. Nuclear Scalar Spin ± Spin Coupling Reveals Novel Properties of Low-Barrier Hydrogen Bonds in a Polar Environment. *Chem. Eur. J.* **1999**, *5*, 492–497. [CrossRef]
72. Shenderovich, I.G.; Smirnov, S.N.; Denisov, G.S.; Gindin, V.A.; Golubev, N.S.; Dunger, A.; Reibke, R.; Kirpekar, S.; Malkina, O.L.; Limbach, H.H. Nuclear Magnetic Resonance of Hydrogen Bonded Clusters between F- and (HF)n: Experiment and Theory. *Ber. Bunsenges. Phys. Chem.* **1998**, *102*, 422–428. [CrossRef]
73. Shenderovich, I.G.; Tolstoy, P.M.; Golubev, N.S.; Smirnov, S.N.; Denisov, G.S.; Limbach, H.H. Low-Temperature NMR Studies of the Structure and Dynamics of a Novel Series of Acid-Base Complexes of HF with Collidine Exhibiting Scalar Couplings Across Hydrogen Bonds. *J. Am. Chem. Soc.* **2003**, *125*, 11710–11720. [CrossRef] [PubMed]
74. Muegge, I.; Heald, S.L.; Brittelli, D. Simple Selection Criteria for Drug-like Chemical Matter. *J. Med. Chem.* **2001**, *44*, 1841–1846. [CrossRef] [PubMed]
75. Smart, B.E. Fluorine substituent effects (on bioactivity). *J. Fluor. Chem.* **2001**, *109*, 3–11. [CrossRef]
76. Chopra, D.; Row, T.N.G. Role of organic fluorine in crystal engineering. *CrystEngComm* **2011**, *13*, 2175–2186. [CrossRef]
77. Desiraju, G.R. Crystal Engineering: From Molecule to Crystal. *J. Am. Chem. Soc.* **2013**, *135*, 9952–9967. [CrossRef] [PubMed]

78. Reichenbacher, K.; Suss, H.I.; Hulliger, J. Fluorine in crystal engineering—"the little atom that could". *Chem. Soc. Rev.* **2005**, *34*, 22–30. [CrossRef] [PubMed]
79. Berger, R.; Resnati, G.; Metrangolo, P.; Weber, E.; Hulliger, J. Organic fluorine compounds: a great opportunity for enhanced materials properties. *Chem. Soc. Rev.* **2011**, *40*, 3496–3508. [CrossRef] [PubMed]
80. Abeles, R.H.; Alston, T.A. A Rationale for the Design of an Inhibitor of Tyrosyl Kinase*. *J. Biol. Chem.* **1990**, *265*, 16705–16708. [PubMed]
81. Chapeau, M.C.; Frey, P.A. Synthesis of UDP-4-deoxy-4-fluoroglucose and UDP-4-deoxy-4-fluorogalactose and Their Interactions with Enzymes of Nucleotide Sugar Metabolism. *J. Org. Chem.* **1994**, *59*, 6994–6998. [CrossRef]
82. Kovacs, T.; Pabuccuoglu, A.; Lesiak, K.; Torrence, P.F. Fluorodeoxy Sugar Analogues of 2′,5′-Oligoadenylates as Probes of Hydrogen Bonding in Enzymes of the 2-5A System. *Bioorg. Chem.* **1993**, *21*, 192–208. [CrossRef]
83. O'Hagan, D.; Rzepa, H.S. Some influences of fluorine in bioorganic chemistry. *Chem. Commun.* **1997**, 645–652. [CrossRef]
84. Takahashi, L.H.; Radhakrishnan, R.; Rosenfield, R.E.; Meyer, E.F.; Trainor, D.A. Crystal Structure of the Covalent Complex Formed by a Peptidyl α,α-Difluoro-β-keto Amide with Porcine Pancreatic Elastase at 1.78-Å Resolution. *J. Am. Chem. Soc.* **1989**, *111*, 3368–3374. [CrossRef]
85. Banerjee, R.; Desiraju, G.R.; Mondal, R.; Howard, J.A.K. Organic Chlorine as a Hydrogen-Bridge Acceptor: Evidence for the Existence of Intramolecular O-H···Cl-C Interactions in Some *gem*-Alkynols. *Chem. Eur. J.* **2004**, *10*, 3373–3383. [CrossRef] [PubMed]
86. Li, C.; Ren, S.F.; Hou, J.L.; Yi, H.P.; Zhu, S.Z.; Jiang, X.K.; Li, Z.T. F···H-N Hydrogen Bonding Driven Foldamers: Efficient Receptors for Dialkylammonium Ions**. *Angew. Chem. Int. Ed.* **2005**, *44*, 5725–5729. [CrossRef] [PubMed]
87. Mido, Y.; Okuno, T. The Intramolecular NH···Cl Hydrogen Bond in Urea Derivatives Containing the O-Chlorophenyl Group. *J. Mol. Struct.* **1982**, *82*, 29–34. [CrossRef]
88. Johnson, E.R.; Keinan, S.; Mori-Sánchez, P.; Contreras-García, J.; Cohen, A.J.; Yang, W. Revealing Noncovalent Interactions. *J. Am. Chem. Soc.* **2010**, *132*, 6498–6506. [CrossRef] [PubMed]
89. Lu, T.; Chen, F. Multiwfn: A Multifunctional Wavefunction Analyzer. *J. Comput. Chem.* **2012**, *33*, 580–592. [CrossRef] [PubMed]
90. Humphrey, W.; Dalke, A.; Schulten, K. VMD: Visual Molecular Dynamics. *J. Mol. Graph.* **1996**, *14*, 33–38. [CrossRef]
91. Bader, R.F.W. *Atoms in Molecules: A Quantum Theory*; Oxford University Press: Oxford, UK, 1990.
92. Bader, R.F.W.; Anderson, S.G.; Duke, A.J. Quantum Topology of Molecular Charge Distributions, 1. *J. Am. Chem. Soc.* **1979**, *101*, 1389–1395. [CrossRef]
93. Bader, R.F.W.; Essén, H. The characterization of atomic interactions. *J. Chem. Phys.* **1984**, *80*, 1943–1960. [CrossRef]
94. Bader, R.F.W.; Nguyen-Dang, T.T.; Tal, Y. A topological theory of molecular structure. *Rep. Prog. Phys.* **1981**, *44*, 893–948. [CrossRef]
95. Runtz, G.R.; Bader, R.F.W.; Messer, R.R. Definition of bond paths and bond directions in terms of the molecular charge distribution. *Can. J. Chem.* **1977**, *55*, 3040–3045. [CrossRef]
96. Espinosa, E.; Molins, E.; Lecomte, C. Hydrogen bond strengths revealed by topological analyses of experimentally observed electron densities. *Chem. Phys. Lett.* **1998**, *285*, 170–173. [CrossRef]
97. Fermi, E.; Pasta, J.; Ulam, S. Studies of Nonlinear Problems. I, Los Alamos Report LA-1940. Los Alamos Scientific Laboratory of the University of California: Oakland, CA, USA, 1955.
98. Chopra, D.; Guru Row, T.N. Evaluation of the interchangeability of C–H and C–F groups: insights from crystal packing in a series of isomeric fluorinated benzanilides. *Cryst. Eng. Comm.* **2008**, *10*, 54–67. [CrossRef]
99. Böhm, H.J.; Banner, D.; Bendels, S.; Kansy, M.; Kuhn, B.; Müller, K.; Obst-Sander, U.; Stahl, M. Fluorine in Medicinal Chemistry. *Chem. Biochem.* **2004**, *5*, 637–643. [CrossRef] [PubMed]
100. Wickenden, O.; Gross, M.F.; Smith, G.A.M. Benzanilides as Potassium Channel Openers. U.S. Patent 6,989,398, 24 January 2006.
101. Calderone, V.; Fiamingo, F.L.; Giorgi, I.; Leonardi, M.; Livi, O.; Martelli, A.; Martinotti, E. Heterocyclic analogs of benzanilide derivatives as potassium channel activators, IX. *Eur. J. Med. Chem.* **2006**, *41*, 761–767. [CrossRef] [PubMed]

102. Biagi, G.; Giorgi, I.; Livi, O.; Nardi, A.; Calderone, V.; Martelli, A.; Martinotti, E.; Salerni, O.L. Synthesis and biological activity of novel substituted benzanilides as potassium channel activators, V. *Eur. J. Med. Chem.* **2004**, *39*, 491–498. [CrossRef] [PubMed]
103. Bondiwell, W.E.; Chan, J.A. Substituted Benzanilides as CCR5 Receptors Ligands, Anti-inflammatory Agents and Antiviral Agents. U.S. Patent 6,515,027, 4 February 2003.
104. Reddy, G.N.M.; Vasantha Kumar, M.V.; Guru Row, T.N.; Suryaprakash, N. N–H···F hydrogen bonds in fluorinated benzanilides: NMR and DFT study. *Phys. Chem. Chem. Phys.* **2010**, *12*, 13232–13237. [CrossRef] [PubMed]
105. Smirnov, S.N.; Golubev, N.S.; Denisov, G.S.; Benedict, H.; Schah-Mohammedi, P.; Limbach, H.H. Hydrogen/Deuterium Isotope Effects on the NMR Chemical Shifts and Geometries of Intermolecular Low-Barrier Hydrogen-Bonded Complexes. *J. Am. Chem. Soc.* **1996**, *118*, 4094–4101. [CrossRef]
106. Golubev, N.S.; Smirnov, S.N.; Gindin, V.A.; Denisov, G.S.; Benedict, H.; Limbach, H.H. Formation of Charge Relay Chains between Acetic Acid and Pyridine Observed by Low-Temperature Nuclear Magnetic Resonance. *J. Am. Chem. Soc.* **1994**, *116*, 12055–12056. [CrossRef]
107. Golubev, N.S.; Denisov, G.S.; Smirnov, S.N.; Shchepkin, D.N.; Limbach, H.H. Evidence by NMR of Temperature-dependent Solvent Electric Field Effects on Proton Transfer and Hydrogen Bond Geometries. *Z. Phys. Chem.* **1996**, *196*, 73–84. [CrossRef]
108. Borman, S. Speedy Route to Folded DNA. *Chem. Eng. News* **1999**, *77*, 36–38. [CrossRef]
109. Dingley, A.J.; Grzesiek, S. Direct Observation of Hydrogen Bonds in Nucleic Acid Base Pairs by Internucleotide $^{2}J_{NN}$ Couplings. *J. Am. Chem. Soc.* **1998**, *120*, 8293–8297. [CrossRef]
110. Pervushin, K.; Ono, A.; Fernández, C.; Szyperski, T.; Kainosho, M.; Wüthrich, K. NMR scalar couplings across Watson–Crick base pair hydrogen bonds in DNA observed by transverse relaxation-optimized spectroscopy. *Proc. Natl. Acad. Sci. USA* **1998**, *95*, 14147–14151. [CrossRef] [PubMed]
111. Fritz, H.; Winkler, T.; Küng, W. Weitreichende Kernspin-Kopplungen in 2-Fluorbenzamiden II. [^{15}N]-2-Fluorbenzamid. *Helv. Chim. Acta* **1975**, *58*, 1822–1824. [CrossRef]
112. Hennig, L.; Ayala-Leon, K.; Angulo-Cornejo, J.; Richter, R.; Beyer, L. Fluorine hydrogen short contacts and hydrogen bonds in substituted benzamides. *J. Fluor. Chem.* **2009**, *130*, 453–460. [CrossRef]
113. Pople, J.A.; Schneider, W.G.; Bernstein, H.J. *High Resolution Nuclear Magnetic Resonance*; McGraw Hill: New York, NY, USA, 1959.
114. Günther, H. *NMR Spectroscopy: Basic Principles, Concepts and Applications in Chemistry*; John Wiley & Sons: New York, NY, USA, 1995.
115. Reddy, G.N.M.; Row, T.N.G.; Suryaprakash, N. Discerning the degenerate transitions of scalar coupled ^{1}H NMR spectra: Correlation and resolved techniques at higher quantum. *J. Magn. Reson.* **2009**, *196*, 119–126. [CrossRef] [PubMed]
116. Bikash, B.; Reddy, G.N.M.; Uday, R.P.; Row, T.N.G.; Suryaprakash, N. Simplifying the Complex ^{1}H-NMR Spectra of Fluorine-Substituted Benzamides by Spin System Filtering and Spin-State Selection: Multiple-Quantum-Single-Quantum Correlation. *J. Phys. Chem. A* **2008**, *112*, 10526–10532.
117. Reddy, G.N.M.; Caldarelli, S. Demixing of Severely Overlapping NMR Spectra through Multiple-Quantum NMR. *Anal. Chem.* **2010**, *82*, 3266–3269.
118. Becke, A.D. Density-functional thermochemistry. III. The role of exact exchange. *J. Chem. Phys.* **1993**, *98*, 5648–5652. [CrossRef]
119. Foresman, J.B.; Keith, T.A.; Wiberg, K.B.; Snoonian, J.; Frisch, M.J. Solvent Effects. 5. Influence of Cavity Shape, Truncation of Electrostatics, and Electron Correlation on ab Initio Reaction Field Calculations. *J. Phys. Chem.* **1996**, *100*, 16098–16104. [CrossRef]
120. Chaudhari, S.R.; Mogurampelly, S.; Suryaprakash, N. Engagement of CF_3 Group in N−H···F−C Hydrogen Bond in the Solution State: NMR Spectroscopy and MD Simulation Studies. *J. Phys. Chem. B* **2013**, *117*, 1123–1129. [CrossRef] [PubMed]
121. Schneider, H.J. Hydrogen bonds with fluorine. Studies in solution, in gas phase and by computations, conflicting conclusions from crystallographic analyses. *Chem. Sci.* **2012**, *3*, 1381–1394. [CrossRef]
122. Jiang, J.C.; Tsa, M.H. Ab Initio Study of the Hydrogen Bonding between Pyrrole and Hydrogen Fluoride: A Comparison of NH···F and FH···π Interactions. *J. Phys. Chem. A* **1997**, *101*, 1982–1988. [CrossRef]

123. Wu, X.; Wang, S. Folding Studies of a Linear Pentamer Peptide Adopting a Reverse Turn Conformation in Aqueous Solution through Molecular Dynamics Simulation. *J. Phys. Chem. B* **2000**, *104*, 8023–8034. [CrossRef]
124. Pophristic, V.; Vemparala, S.; Ivanov, I.; Liu, Z.; Klein, M.L.; DeGrado, W.F. Controlling the Shape and Flexibility of Arylamides: A Combined ab Initio, ab Initio Molecular Dynamics, and Classical Molecular Dynamics Study. *J. Phys. Chem. B* **2006**, *110*, 3517–3526. [CrossRef] [PubMed]
125. Schnabel, T.; Srivastava, A.; Vrabec, J.; Hasse, H. Hydrogen Bonding of Methanol in Supercritical CO_2: Comparison between ^{1}H NMR Spectroscopic Data and Molecular Simulation Results. *J. Phys. Chem. B* **2007**, *111*, 9871–9878. [CrossRef] [PubMed]
126. Liu, Z.; Remsing, R.C.; Liu, D.; Moyna, G.; Pophristic, V. Hydrogen Bonding in *ortho*-Substituted Arylamides: The Influence of Protic Solvents. *J. Phys. Chem. B* **2009**, *113*, 7041–7044. [CrossRef] [PubMed]
127. Galan, J.F.; Brown, J.; Wildin, J.L.; Liu, Z.; Liu, D.; Moyna, G.; Pophristic, V. Intramolecular Hydrogen Bonding in *ortho*-Substituted Arylamide Oligomers: A Computational and Experimental Study of *ortho*-Fluoro- and *ortho*-Chloro-*N*-methylbenzamides. *J. Phys. Chem. B.* **2009**, *113*, 12809–12815. [CrossRef] [PubMed]
128. International Union of Pure and Applied Chemistry (IUPAC). *Compendium of Chemical Terminology*, 2nd ed.; The "Gold Book"; McNaught, A.D., Wilkinson, A., Eds.; Blackwell Scientific Publications: Oxford, UK, 1997.
129. Friedman, L.; Litle, R.L.; Reichle, W.R. *p*-Toluenesulphonylhydrazide [*p*-Toluenesulphonic acid, hydrazide]. *Org. Synth.* **1960**, *40*, 93–96.
130. Mohareb, R.M.; Fleita, D.H.; Sakka, O.K. Novel Synthesis of Hydrazide-Hydrazone Derivatives and Their Utilization in the Synthesis of Coumarin, Pyridine, Thiazole and Thiophene Derivatives with Antitumor Activity. *Molecules* **2011**, *16*, 16–27. [CrossRef] [PubMed]
131. Wadrdakhan, W.W.; El-saeed, N.N.E.; Mohereb, R.M. Development of coated beads for oral controlled delivery of cefaclor: In vitro evaluation. *Acta Pharm.* **2013**, *63*, 45–57.
132. Swietlińska, Z.; Zuk, J. Cytotoxic Effects of Maleic Hydrazide. *Mutat. Res. Rev. Gen. Toxicol.* **1978**, *55*, 15–30. [CrossRef]
133. Kaplancikli, Z.A.; Turan-Zitouni, G.; Ozdemir, A.; Teulade, J.C. Synthesis and Antituberculosis Activity of New Hydrazide Derivatives. *Arch. Pharm.* **2008**, *341*, 721–724. [CrossRef] [PubMed]
134. Mishra, S.K.; Suryaprakash, N. Intramolecular hydrogen bonds involving organic fluorine in the derivatives of hydrazides: an NMR investigation substantiated by DFT based theoretical calculations. *Phys. Chem. Chem. Phys.* **2015**, *17*, 15226–15235. [CrossRef] [PubMed]
135. Kohn, W.; Sham, L.J. Self-Consistent Equations Including Exchange and Correlation Effects. *Phys. Rev.* **1965**, *140*, A1133–A1138. [CrossRef]
136. Parr, R.G.; Yang, W. *Density-Functional Theory of Atoms and Molecules*; Oxford University Press: New York, NY, USA, 1989.
137. Morris, K.F.; Johnson, C.S. Diffusion-Ordered Two-Dimensional Nuclear Magnetic Resonance Spectroscopy. *J. Am. Chem. Soc.* **1992**, *114*, 3139–3141. [CrossRef]
138. Morris, K.F.; Johnson, C.S. Resolution of Discrete and Continuous Molecular Size Distributions by Means of Diffusion-Ordered 2D NMR Spectroscopy. *J. Am. Chem. Soc.* **1993**, *115*, 4291–4299. [CrossRef]
139. Reed, A.E.; Curtiss, L.A.; Weinhold, F. Intermolecular Interactions from a Natural Bond Orbital, Donor-Acceptor Viewpoint. *Chem. Rev.* **1988**, *88*, 899–926. [CrossRef]
140. Axenrod, T.; Pregosin, P.S.; Wieder, M.J.; Becker, E.D.; Bradley, R.B.; Milne, G.W.A. Nitrogen- 15 Nuclear Magnetic Resonance Spectroscopy. Substituent Effects on ^{15}N-H Coupling Constants and Nitrogen Chemical Shifts in Aniline Derivatives. *J. Am. Chem. Soc.* **1971**, *93*, 6536–6541. [CrossRef]
141. Dunger, A.; Limbach, H.-H.; Weisz, K. Geometry and Strength of Hydrogen Bonds in Complexes of 2′-Deoxyadenosine with 2′-Deoxyuridine. *J. Am. Chem. Soc.* **2000**, *122*, 10109–10114. [CrossRef]
142. Grzesiek, S.; Cordier, F.; Jaravine, V.; Barfield, M. Insights into biomolecular hydrogen bonds from hydrogen bond scalar couplings. *Prog. Nucl. Magn. Reson. Spectrosc.* **2004**, *45*, 275–300. [CrossRef]
143. Afonin, A.V.; Ushakov, I.A.; Sobenina, L.N.; Stepanova, Z.V.; Petrova, O.G.V.; Trofimov, B.A. Different types of hydrogen bonds in 2-substituted pyrroles and 1-vinyl pyrroles as monitored by ^{1}H, ^{13}C and ^{15}N NMR spectroscopy and ab initio calculations. *Magn. Reson. Chem.* **2006**, *44*, 59–65. [CrossRef] [PubMed]
144. King, M.M.; Yeh, H.J.C.; Dudek, G.O. Nitrogen NMR Spectroscopy: Application to some Substituted Pyrroles. *Org. Magn. Reson.* **1976**, *8*, 208–212. [CrossRef]
145. Cheeseman, J.R.; Trucks, G.W.; Keith, T.A.; Frisch, M.J. A comparison of models for calculating nuclear magnetic resonance shielding tensors. *J. Chem. Phys.* **1996**, *104*, 5497–5509. [CrossRef]

146. Nakahara, M.; Wakai, C. Monomeric and Cluster States of Water Molecules in Organic Solvent. *Chem. Lett.* **1992**, *21*, 809–812. [CrossRef]
147. Vizioli, C.; de Azua, M.C.R.; Giribet, C.G.; Contreras, R.H.; Turi, L.; Dannenberg, J.J.; Rae, I.D.; Weigold, J.A.; Malagoli, M. Proximity Effects on Nuclear Spin-Spin Coupling Constants. 1. ^{1}J(CH) Couplings in the Vicinity of an Atom Bearing Lone Pairs. *J. Phys. Chem.* **1994**, *98*, 8858–8861. [CrossRef]
148. Lakshmipriya, A.; Suryaprakash, N. Two- and Three-Centered Hydrogen Bonds Involving Organic Fluorine Stabilize Conformations of Hydrazide Halo Derivatives: NMR, IR, QTAIM, NCI, and Theoretical Evidence. *J. Phys. Chem. A* **2016**, *120*, 7810–7816. [CrossRef] [PubMed]
149. Walter, W.W.; Michael, H.A. *"Polyimides" in Ullmann's Encyclopedia of Industrial Chemistry*; Wiley-VCH: Weinheim, Germany, 2002.
150. Prinos, J.; Tselios, C.; Bikiaris, D.; Panayiotou, C. Properties of miscible blends of polyglutarimide with poly(styrene-co-maleic anhydride). *Polymer* **1997**, *38*, 5921–5930. [CrossRef]
151. Luo, L.; Zheng, Y.; Huang, J.; Li, K.; Wang, H.; Feng, Y.; Wang, X.; Liu, X. High-performance copoly(benzimidazole-benzoxazole-imide) fibers: Fabrication, structure, and properties. *J. Appl. Polym. Sci.* **2015**, *132*. [CrossRef]
152. Kanaoka, Y. Photoreactions of Cyclic Imides. Examples of Synthetic Organic Photochemistry. *Acc. Chem. Res.* **1978**, *11*, 407–413. [CrossRef]
153. Stec, J.; Huang, Q.; Pieroni, M.; Kaiser, M.; Fomovska, A.; Mui, E.; Witola, W.H.; Bettis, S.; McLeod, R.; Brun, R.; Kozikowski, A.P. Synthesis, Biological Evaluation, and Structure−Activity Relationships of N-Benzoyl-2-hydroxybenzamides as Agents Active against *P. falciparum* (K1 strain), *Trypanosomes*, and *Leishmania*. *J. Med. Chem.* **2012**, *55*, 3088–3100. [CrossRef] [PubMed]
154. Wang, H.; Kelley, S.P.; Brantley, J.W.; Chatel, G.; Shamshina, J.; Pereira, J.F.B.; Debbeti, V.; Myerson, A.S.; Rogers, R.D. Ionic Fluids Containing Both Strongly and Weakly Interacting Ions of the Same Charge Have Unique Ionic and Chemical Environments as a Function of Ion Concentration. *ChemPhysChem* **2015**, *16*, 993–1002. [CrossRef] [PubMed]
155. Sprecher, D.; Maxwell, M.; Goodman, J.; White, B.; Tang, C.M.; Boullay, V.; de Gouville, A.C. Discovery and characterization of GSK256073, a non-flushing hydroxy-carboxylic acid receptor 2 (HCA2) agonist. *Eur. J. Pharmacol.*, **2015**, *756*, 1–7. [CrossRef] [PubMed]
156. Mhidia, R.; Boll, E.; Fécourt, F.; Ermolenko, M.; Ollivier, N.; Sasaki, K.; Crich, D.; Delpech, B.; Melnyk, O. Exploration of an imide capture/*N*,*N*-acyl shift sequence for asparagine native peptide bond formation. *Bioorg. Med. Chem.* **2013**, *21*, 3479–3485. [CrossRef] [PubMed]
157. Li, Y.; Wang, Y.; Wang, J. Microwave-Assisted Synthesis of Amides from Various Amines and Benzoyl Chloride under Solvent-Free Conditions: A Rapid and Efficient Method for Selective Protection of Diverse Amines. *Russ. J. Organ. Chem.* **2008**, *44*, 358–361. [CrossRef]
158. Mishra, S.K.; Suryaprakash, N. Organic fluorine involved intramolecular hydrogen bonds in the derivatives of imides: NMR evidence corroborated by DFT based theoretical calculations. *RSC Adv.* **2015**, *5*, 86013–86022. [CrossRef]
159. Contreras-García, J.; Yang, W.; Johnson, E.R. Analysis of Hydrogen-Bond Interaction Potentials from the Electron Density: Integration of Noncovalent Interaction Regions. *J. Phys. Chem. A* **2011**, *115*, 12983–12990. [CrossRef] [PubMed]
160. Gellman, S.H.; Adams, B.R.; Dado, G.P. Temperature-Dependent Changes in the Folding Pattern of a Simple Triamide. *J. Am. Chem. Soc.* **1990**, *112*, 460–461. [CrossRef]
161. Gellman, S.H.; Dado, G.P.; Liang, G.B.; Adams, B.R. Conformation-Directing Effects of a Single Intramolecular Amide-Amide Hydrogen Bond: Variable-Temperature NMR and IR Studies on a Homologous Diamide Series. *J. Am. Chem. Soc.* **1991**, *113*, 1164–1173. [CrossRef]
162. Martinez-Martinez, F.J.; Ariza-Castolo, A.; Tlahuext, H.; Tlahuextl, M.; Contreras, R. ^{1}H, ^{13}C, ^{15}N, 2D and Variable Temperature NMR Study of the Role of Hydrogen Bonding in the Structure and Conformation of Oxamide Derivatives. *J. Chem. Soc. Perkin Trans. 2* **1993**, 1481–1485. [CrossRef]
163. Rinaldi, P.L. Heteronuclear 2D-NOE Spectroscopy. *J. Am. Chem. Soc.* **1983**, *105*, 5167–5168. [CrossRef]
164. Yu, C.; Levy, G.C. Solvent and Intramolecular Proton Dipolar Relaxation of the Three Phosphates of ATP: A Heteronuclear 2D NOE Study. *J. Am. Chem. Soc.* **1983**, *105*, 6994–6996. [CrossRef]
165. Yu, C.; Levy, G.C. Two-Dimensional Heteronuclear NOE (HOESY) Experiments: Investigation of Dipolar Interactions between Heteronuclei and Nearby Protons. *J. Am. Chem. Soc.* **1984**, *106*, 6533–6537. [CrossRef]

166. Lakshmipriya, A.; Chaudhari, S.R.; Shahi, A.; Arunan, E.; Suryaprakash, N. Three centered hydrogen bonds of the type C-O···H(N)···X–C in diphenyloxamide derivatives involving halogens and a rotating CF_3 group: NMR, QTAIM, NCI and NBO studies. *Phys. Chem. Chem. Phys.* **2015**, *17*, 7528–7536. [CrossRef] [PubMed]
167. Shahi, A.; Arunan, E. Hydrogen bonding, halogen bonding and lithium bonding: an atoms in molecules and natural bond orbital perspective towards conservation of total bond order, inter- and intra-molecular bonding. *Phys. Chem. Chem. Phys.* **2014**, *16*, 22935–22952. [CrossRef] [PubMed]
168. Brotherhood, P.R.; Luck, I.J.; Blake, I.M.; Jensen, P.; Turner, P.; Crossley, M.J. Regioselective Reactivity of an Asymmetric Tetravalent Di[dihydroxotin(IV)] Bis-Porphyrin Host Driven by Hydrogen-Bond Templation. *Chem. Eur. J.* **2008**, *14*, 10967–10977. [CrossRef] [PubMed]
169. Mishra, S.K.; Suryaprakash, N. Study of H/D exchange rates to derive the strength of intramolecular hydrogen bonds in halo substituted organic building blocks: An NMR spectroscopic investigation. *Chem. Phys. Letts.* **2015**, *639*, 254–260. [CrossRef]
170. Pietrzak, M.; Limbach, H.H.; Torralba, M.P.; Sanz, D.; Claramunt, R.M.; Elguero, J. Scalar Coupling Constants Across the Intramolecular NHN-Hydrogen Bond of Symmetrically and Non-symmetrically substituted 6-Aminofulvene-1-aldimines. *Magn. Reson. Chem.* **2001**, *39*, S100–S108. [CrossRef]
171. Shenderovich, I.G.; Burtsev, A.P.; Denisov, G.S.; Golubev, N.S.; Limbach, H.H. Influence of the temperature-dependent dielectric constant on the H/D isotope effects on the NMR chemical shifts and the hydrogen bond geometry of the collidine–HF complex in $CDF_3/CDClF_2$ solution. *Magn. Reson. Chem.* **2001**, *39*, S91–S99. [CrossRef]
172. Wang, Y.X.; Marquardt, J.L.; Wingfield, P.; Stahl, S.J.; Huang, S.L.; Torchia, D.; Bax, A. Simultaneous Measurement of ^{1}H-^{15}N, ^{1}H-^{13}C′, and ^{15}N-^{13}C′ Dipolar Couplings in a Perdeuterated 30 kDa Protein Dissolved in a Dilute Liquid Crystalline Phase. *J. Am. Chem. Soc.* **1998**, *120*, 7385–7386. [CrossRef]
173. Cornilescu, G.; Hu, J.S.; Bax, A. Identification of the Hydrogen Bonding Network in a Protein by Scalar Couplings. *J. Am. Chem. Soc.* **1999**, *121*, 2949–2950. [CrossRef]
174. Norwood, T.J. Multiple-Quantum NMR Methods. *Prog. NMR Spect.* **1992**, *24*, 295–375. [CrossRef]
175. Bodenhausen, G. Multiple-Quantum NMR. *Prog. NMR Spect.* **1981**, *14*, 137–173. [CrossRef]
176. Divya, K.; Hebbar, S.; Suryaprakash, N. Intra-molecular hydrogen bonding with organic fluorine in the solution state: Deriving evidence by a two dimensional NMR experiment. *Chem. Phys. Lett.* **2012**, *525–526*, 129–133. [CrossRef]
177. Hebbar, S.; Suryaprakash, N. Spin-selective multiple quantum excitation: Relative signs of the couplings and ambiguous situations. *J. Magn. Reson.* **2008**, *194*, 192–201. [CrossRef] [PubMed]
178. Munowitz, M.; Pines, A. Homogeneous NMR spectra in inhomogeneous fields. *Science* **1986**, *233*, 525–531. [CrossRef] [PubMed]
179. Bikash, B.; Suryaprakash, N. Spin selective multiple quantum NMR for spectral simplification, determination of relative signs, and magnitudes of scalar couplings by spin state selection. *J. Chem. Phys.* **2007**, *127*, 214510–214521.
180. Griffey, R.H.; Poulter, C.D.; Bax, A.; Hawkins, B.L.; Yamaizumi, Z.; Nishimura, S. Multiple quantum two-dimensional ^{1}H- ^{15}N nuclear magnetic resonance spectroscopy: Chemical shift correlation maps for exchangeable imino protons of *Escherichia coli* $tRNA_f^{Met}$ in water. *Proc. Nat. Acad. Sci. USA* **1983**, *80*, 5895–5897. [CrossRef] [PubMed]
181. Frisch, M.J.; Trucks, G.W.; Schlegel, H.B.; Scuseria, G.E.; Robb, M.A.; Cheeseman, J.R.; Scalmani, G.; Barone, V.; Mennucci, B.; Petersson, G.A.; et al. *Gaussian G09*; Gaussian, Inc.: Wallingford, CT, USA, 2009.
182. Phillips, J.C.; Braun, R.; Wang, W.; Gumbart, J.; Tajkhorshid, E.; Villa, E.; Chipot, C.; Skeel, R.D.; Kale, L.; Schulten, K. Scalable Molecular Dynamics with NAMD. *J. Comput. Chem.* **2005**, *26*, 1781–1802. [CrossRef] [PubMed]
183. Darden, T.; York, D.; Pedersen, L. Particle mesh Ewald: An N·log(N) method for Ewald sums in large systems. *J. Chem. Phys.* **1993**, *98*, 10089–10092. [CrossRef]
184. Keith, T.A. *AIMAll (Version 13.11.04)*; TK Gristmill Software: Overland Park, KS, USA, 2013.
185. Takemura, H.; Kon, N.; Yasutake, M.; Nakashima, S.; Shinmyozu, T.; Inazu, T. The C-F···Cation Interaction: An Ammonium Complex of a Hexafluoro Macrocyclic Cage Compound. *Chem. Eur. J.* **2000**, *6*, 2334–2337. [CrossRef]

186. Zhao, X.; Wang, X.Z.; Jiang, X.K.; Chen, Y.Q.; Li, Z.T.; Chen, G.J. Hydrazide-Based Quadruply Hydrogen-Bonded Heterodimers. Structure, Assembling Selectivity, and Supramolecular Substitution. *J. Am. Chem. Soc.* **2003**, *125*, 15128–15139. [CrossRef] [PubMed]
187. Schaftenaar, G.; Noordik, J.H. Molden: A pre- and post-processing program for molecular and electronic structures. *J. Comput. Aided Mol. Des.* **2000**, *14*, 123–134. [CrossRef] [PubMed]